Bioactive Materials 6 (2021) 1051–1072

Contents lists available at ScienceDirect

Bioactive Materials

journal homepage: http://www.keaipublishing.com/biomat

Recruited CD68$^+$CD206$^+$ macrophages orchestrate graft immune tolerance to prompt xenogeneic-dentin matrix-based tooth root regeneration

Hui Li[a,b,c,d], Jingjing Sun[a,b,c,e], Hefeng Yang[b,f], Xue Han[a,b,g], Xiangyou Luo[a,b,c], LiJun Liao[a,b,g], Bo Yang[a,b,c], Tian Zhu[a,b,g], Fangjun Huo[b], Weihua Guo[a,b,g,*], Weidong Tian[a,b,c,**]

[a] State Key Laboratory of Oral Diseases, West China Hospital of Stomatology, Sichuan University, Chengdu, China
[b] National Engineering Laboratory for Oral Regenerative Medicine, West China Hospital of Stomatology, Sichuan University, Chengdu, China
[c] Department of Oral and Maxillofacial Surgery, West China Hospital of Stomatology, Sichuan University, Chengdu, China
[d] Department of Stomatology, Beijing Shijitan Hospital, Capital Medical University, Beijing, China
[e] Department of Stomatology, The First Affiliated Hospital of Zhengzhou University, Zhengzhou, China
[f] Department of Dental Research, The Affiliated Stomatological Hospital of Kunming Medical University, Kunming, China
[g] Department of Pediatric Dentistry, West China Hospital of Stomatology, Sichuan University, Chengdu, China

ARTICLE INFO

Keywords:
Xenogeneic extracellular matrix
Macrophage polarization
Cellular response
Organ regeneration
Parenchymal and stromal tissues regeneration

ABSTRACT

Successful regenerative medicine strategies of xenogeneic extracellular matrix need a synergistic balance among inflammation, fibrosis, and remodeling process. Adaptive macrophage subsets have been identified to modulate inflammation and orchestrate the repair of neighboring parenchymal tissues. This study fabricated PPARγ-primed CD68$^+$CD206$^+$ M2 phenotype (M2γ), and firstly verified their anti-inflammatory and tissue-regenerating roles in xenogeneic bioengineered organ regeneration. Our results showed that Th1-type CD3$^+$CD8$^+$ T cell response to xenogeneic-dentin matrix-based bioengineered root complex (xeno-complex) was significantly inhibited by M2γ macrophage *in vitro*. PPARγ activation also timely recruited CD68$^+$CD206$^+$ tissue macrophage polarization to xeno-complex *in vivo*. These subsets alleviated proinflammatory cytokines (TNF-α, IFN-γ) at the inflammation site and decreased CD3$^+$CD8$^+$ T lymphocytes in the periphery system. When translated to an orthotopic nonhuman primate model, PPARγ-primed M2 macrophages immunosuppressed IL-1β, IL-6, TNF-α, MMPs to enable xeno-complex to effectively escape immune-mediated rejection and initiate graft-host synergistic integrity. These collective activities promoted the differentiation of odontoblast-like and periodontal-like cells to guide pulp-dentin and cementum-PDLs-bone regeneration and rescued partially injured odontogenesis such as DSPP and periostin expression. Finally, the regenerated root showed structure-biomechanical and functional equivalency to the native tooth. The timely conversion of M1-to-M2 macrophage mainly orchestrated odontogenesis, fibrogenesis, and osteogenesis, which represents a potential modulator for intact parenchymal-stromal tissue regeneration of targeted organs.

1. Introduction

De-novo organogenesis, have been successfully addressed by autologous bioengineered extracellular matrix (ECM) [1], but generalized clinical applications are confined to donor shortage. The naturally occurring xenografts or xenogeneic matrix, delivering essential trophic signals, could be favorable replacements [2,3]. Specific-shaped xenogeneic matrix recellularised with allogeneic stem cells to regenerate organs is a promising strategy. Generally, these bioengineered organs are transplanted with a goal of parenchymal and stromal tissue regeneration in its natural milieu [4]. Precisely, this de-novo organogenesis model could be offered by the tooth root organ. The special pulp-dentin and cementum-periodontium complexes parallelly contribute to highly-mineralized parenchymal tissues and functional neurovascular stromal components [4].

Regeneration of bioengineered organs needs a synergistic balance

Peer review under responsibility of KeAi Communications Co., Ltd.

* Corresponding author. Department of Pediatric Dentistry, West China School of Stomatology, Sichuan University, No. 14, 3rd Sec., Ren Min Nan Road, Chengdu, 610041, PR China.
** Corresponding author. State Key Laboratory of Oral Diseases, West China Hospital of Stomatology, Sichuan University, No. 14, 3rd Sec., Ren Min Nan Road, Chengdu, 610041, PR China.
E-mail addresses: guoweihua943019@163.com (W. Guo), drtwd@sina.com (W. Tian).

https://doi.org/10.1016/j.bioactmat.2020.09.029
Received 6 August 2020; Received in revised form 23 September 2020; Accepted 29 September 2020

among inflammation, fibrosis and, regenerative program. Decellularization has been proved as an effective tool to reduce the immunogenicity of xenogeneic ECM. In a humanized mice model, both porcine or human-derived decellularized hydrogels induced similar infiltration of T-helper 2 cells [5]. However, the bioengineered ECM is often recognized as a foreign body, so that the host defends itself by extended chronic inflammation and even fibrous encapsulation, resulting in the failing of de-novo organogenesis [6]. Such biological processes are usually initiated by a complex inflammatory response, characterized by the recruitment and activation of neutrophils, natural killer cells, B cells, T cells, macrophages, fibroblasts [7]. All these make up the cellular response that orchestrates the following repair process. When the cellular response is well controlled, an architecture-morphological equivalency to normal tissue could be re-established. However, if the cellular response is dysregulated, the biological process always ends up with chronic inflammation, pathological fibrosis, and even organ failure [8]. With all stages, macrophages exhibit plasticity and adopt pro-inflammatory, pro-wound-healing, pro-fibrotic, anti-inflammatory, anti-fibrotic, and tissue-regenerating phenotypes [9], make it a therapeutic target that might regulate the cellular response to bioengineered organs.

These polarized macrophages phenotypes are generally defined as classically pro-inflammatory M1 phenotype or alternative anti-inflammatory M2 phenotype [10]. Respectively, M1 macrophages accelerate inflammation with intensive release of interleukin 1 beta (IL-1β), tumor necrosis factor-alpha (TNF-α), functioning in host defense systems, and debris clearance. In contrast, M2 macrophages antagonize M1 macrophage responses and govern anti-inflammatory activities by producing interleukin 4 (IL-4), interleukin 13 (IL-13), transforming growth factor-β1 (TGF-β1), and interleukin 10 (IL-10), functioning in wound healing and tissue repair [9,10]. Given this dichotomy in M1/M2 functions, the M1/M2 phenotypic profile at tissue-implants sites is of spotlight interests. It has been reported that the shift to M2 macrophage might predict favorable outcomes of tissue regeneration after ECM transplantation [11]. For instance, the polarization of M2 macrophages in a collagen graft promoted differentiation of Schwann cells, nerve fiber recovery, and blood vessel formation [12]. Additionally, the hierarchical nanointerface implants could repair mandible defects mainly depended on M2 macrophage-mediated osteogenic differentiation [13]. Via various forms, M2 macrophage regulates the synthesis of extracellular matrix (ECM) components, promoting the repair of neighboring parenchymal and stromal tissues [9]. However, it was unclear whether M2 macrophage could perform these effects on a complete xenogeneic organ regeneration of parenchymal and stromal tissues, such as the tooth organ.

Our previous study fabricated decellularized and demineralized dentin matrix derived from porcine, termed as porcine-derived treated dentin matrix (pTDM). When populated with allogeneic dental follicle cells (DFCs), a switch from M1 to M2 macrophage was observed at about 3 weeks after transplantation *in vivo* [14]. The prolonged M1 macrophage at 1–3 weeks inevitably enhanced the risk of chronic inflammation and foreign body response. Parallelly, the present study further reported an enhanced increase of $CD3^+CD8^+$ T cells response triggered by pTDM derived xenogeneic bioengineered tooth root complex (xeno-complex). To antagonize the cellular response and previously reported M1 infiltration, utilizing M2 macrophage polarization as a therapeutic target was firstly proposed in our study. A $CD68^+CD206^+$ M2 phenotype was primed by activation of peroxisome proliferators activate receptors-γ (PPARγ). And both the $CD68^+CD206^+$ M2 macrophage and PPARγ agonist (rosiglitazone, RSG) inhibited the induced Th1-associated $CD3^+CD8^+$ T cells. When translated *in vivo*, the $CD68^+CD206^+$ M2 macrophages were recruited to the peripheral and intracavity of xeno-complex after RSG treatment, with a ratio of M2: M1 > 1 from 3 days to 3 weeks. These subsets alleviated inflammation both at implant sites and in the periphery system. When translated to an orthotopic nonhuman primate model, RSG treatment immunosuppressed IL-1β, IL-6, TNF-α, MMPs, and up-regulated IL-4 to enable the transplanted xeno-complex to effectively escape an immune-mediated rejection. And with the differentiation of odontoblast-like cells and periodontal-like cells, pulp-dentin and cementum-PDLs-bone complexes were regenerated. Positive stained for DMP-1, DSPP, col-1, col-III, periostin, and βtubulinIII, the regenerated parenchymal and stromal tissues also exhibited a structure-biomechanical equivalency to the native tooth root. Finally, our study reported regeneration of xenogeneic bioengineered tooth root with a non-degradable form and maintenance of mechanical properties. Altogether highlight the macrophage polarization as a therapeutic target in xenogeneic ECM based organ regeneration.

2. Materials and methods

All specimens from humans were conducted in accordance with the protocol approved by the West China Hospital of Stomatology Institutional Review Board (WCSHIRB), with informed patient consent as required.

2.1. Fabrication of xenogeneic bioengineered tooth root complex (xeno-complex)

2.1.1. Cells isolation and culture. Human dental follicles were obtained from impacted third molars of healthy young individuals under 18 years old, and 2–3 d neonatal rats were used for rat dental follicles cell (DFCs) isolation. Monkey-derived DFCs (mDFCs) were harvested from a 2∼3-year-old macaque. DFCs were isolated and cultured as described previously [15]. Passages 2–4 were used for the following experiments.

2.1.2. Preparation of porcine treated dentin matrix (pTDM). pTDM was fabricated as described for human TDM previously. Briefly, the incisor teeth were extracted from pigs executed in the morning. The dental pulp tissue, pre-dentin, and periodontal tissue were completely scraped away with a curette. The resulting dentin matrices were processed into a cone shape, approximately with a length of 10 mm, an external diameter of 3–5 mm, and a thickness of 1 mm. The matrices were mechanically washed in deionized water using an ultrasonic cleaner, then treated with gradient demineralization by 17%, 10%, 5% ethylene diamine tetra-acetic acid (EDTA, Sigma-Aldrich, St. Louis, MO, USA), thus leading to complete exposure of dentinal tubules [14,15]. The obtained pTDM were maintained in sterile PBS with 100 units/ml penicillin (HyClone, USA) and 100 mg/ml streptomycin (HyClone, USA) for 72 h, and finally stored in α-MEM at 4 °C. Xeno-complex were constructed via a combination of allogenic DFCs (aDFCs) with pTDM, respectively, by seeding hDFCs/rDFCs/mDFCs on pTDM for 7 days as previously described.

2.2. Immune cells culture and collection of conditioned media

2.2.1. Isolation of hPBMCs

The hPBMCs were isolated from enriched leukocyte fractions of human peripheral blood provided by the Blood Center of Chengdu, Sichuan province using Ficoll density gradient centrifugation (Lymphoprep™, STEMCELL TECHNOLOGIES INC. Canada). hPBMCs were resuspended in RPMI-1640 medium supplemented with 10% FBS and 1% v/v of penicillin-streptomycin mixture.

2.2.2. Culture of monocytes/macrophages

Human monocytes were isolated from enriched leukocyte fractions of human peripheral blood provided by the Chengdu Blood Center using sequential Ficoll and Percoll density gradient centrifugation. The cells were suspended in RPMI 1640 supplemented with 10% human AB serum (GIBCO-BRL, Life Technologies, Grand Island, NY) and 1% v/v of penicillin-streptomycin. Monocytes were seeded at a density of 2×10^6 cells/well in six-well plates and incubated at 37 °C with 5%

CO_2 for 24 h. Non-adherent cells were discarded, and adherent monocyte differentiation in resting macrophages (M0) occurred after 7 days of culture. Alternative activated macrophages (M2) were obtained by stimulating freshly isolated monocytes with human IL-4 (M2a, 15 ng/ml) or the addition of rosiglitazone (M2γ, 100 nM) at the first and third day of M2 differentiation without replacing the medium (M2γ). M2γ macrophages were cultured for 7 days. Then, the medium was removed and cells were cultured for an additional 24 h with fresh medium. The resulting M2γ conditional medium (M2γ medium) was collected for the following experiments.

2.3. Co-culture system of xeno-complex with hPBMCs

2.3.1. CFSE-based assay of immune cell proliferation

To mirror the immune microenvironment, plates (Thermo Fisher Scientific, USA) were coated with a suboptimal dose of monoclonal anti-CD3 antibody (0.025 μg/ml, Biolegend, USA) to obtain a basal stimulation of immune cells for the CFSE-based proliferation assay, which does not induce T cell proliferation or low proliferation rates [16]. The isolated hPBMCs were labeled with a 5 mM stock CFSE solution (Invitrogen, Carlsbad, CA, USA) for a final working concentration of 1 μM. The CFSE-labeled hPBMCs (1.5×10^6) were seeded in anti-CD3-coated 6-well plates and were co-cultured with pTDM or xeno-complex along with a volume of 4 ml/well RPMI-1640 medium (supplemented with 10% FBS and 1% v/v of penicillin-streptomycin mixture). Phytohemagglutinin (PHA, Sigma-Aldrich, USA)-treated cells served as the positive control, and unstimulated CFSE-labeled cells served as the negative control. After 5 days culture in a humidified atmosphere with 5% CO_2 at 37 ˚C, all supernatants of the co-cultures and controls were collected, centrifuged (4 ˚C, 1000×*g*, 5 min), and frozen at 80 ˚C for further cytokine analysis. The cells were harvested, and the proliferation level was measured by flow cytometry.

2.3.2. Flow cytometry

The CFSE-labeled cells were harvested, washed with 1 ml cold PBS (2% FBS), and then stained with mouse anti-human CD3-PerCP-Cy7 (Biolegend, USA), CD4-APC and CD8-PE, (BD Biosciences). Incubation at 4 ˚C was stopped after 30 min and the cells were washed with PBS (2% FBS) twice and resuspended in 300 μl of PBS (2% FBS). The proliferation level was measured by flow cytometry using a BD Accuri™ C6 flow cytometer and analyzed by FlowJo software (Treestar, Inc., San Carlos, CA).

2.3.3. Luminex® multiplex MAP analysis of inflammatory cytokines

The supernatants or M2γ medium were analyzed using MILLIPLEX® MAP Kits (Millipore, Billerica, MA, USA) for inflammation/immunology, including human Th1/Th2 Cytokines (IL-1β, IL-4, IL-5, IL-6, IL-8, IL-13, IL-12, IL-2, IL-10, IFN-γ, TNF-α, HGF, and TGF-β1). Frozen supernatants were thawed and measured by Luminex® Multiplexing Instruments and analyzed by MILLIPLEX® Analyst 5.1 software following the manufacturers' recommendations.

2.3.4. Real-time PCR

Total RNA was extracted from macrophages or non-CFSE-labeled hPBMCs (co-culture system of xeno-complex with non-CFSE-labeled hPBMCs) using RNAiso Plus according to the manufacturer's instructions (TaKaRa Biotechnology, Dalian, China). First-strand cDNA was synthesized from 1 μg of total RNA via the RevertAid First Strand cDNA Synthesis Kit (Thermo Scientific, Pittsburgh, PA, USA). Quantitative PCR was performed using a QuantStudio® 6 Flex Real-Time PCR System (Thermo Scientific, Rockford, IL, USA) with SYBR® Premix Ex Taq™ II (Tli RNaseH Plus) (TaKaRa Biotechnology, Dalian, China) according to the manufacturer's instructions. The expression levels for each gene were normalized to GAPDH (mean ± SEM; n ≥ 3). The primer sequences are listed in Table S1.

2.3.5. Immunofluorescence analysis

Immunofluorescence staining was performed. Briefly, differentiated macrophages (M0, M2a, M2γ) or adhered macrophages in the coculture system (non-CFSE-labeled hPBMCs) were fixed with 4% paraformaldehyde in PBS for 30 min at room temperature and then washed with PBS. Then cells were permeabilized with 0.1%TritonX-100 in PBS and blocked with 1% bovine serum albumin (BSA) for 30min. Primary antibodies (mouse anti-human CD68, rabbit anti-human CCR7/CD206, Abcam, Cambridge, MA, UK) was diluted in PBS containing 1%BSA, and cells incubated in the diluted primary antibodies at 4 ˚C overnight. Then after wash three times by PBS, cells were incubated by anti-mouse Alexa Fluor 488-IgG and anti-rabbit Alexa Fluor 555-IgG (Invitrogen, Carlsbad, CA, USA) for 60 min at room temperature. 4′,6′-diamino-2-phenylindole (DAPI, Biosharp, Hefei, China) was used to stain nuclear. Images were acquired using a Leica DMI6000 B inverted fluorescence microscope (Leica Optical, Wetzlar, Germany).

2.4. Sequential observation in rat subcutaneous model

The animal experiment or specimens were approved by the Research Ethics Committee of West China School of Stomatology and were conducted in WestChina-Frontier PharmaTech.

2.4.1. Rats

Rats were housed in ventilated cages under required conditions with regular food and water supplements. Rats (average weight of 200–250 g) that were 10–12 weeks old were used for experiments. Approximately one hundred Sprague-Dawley (SD) rats were randomly divided into three groups: xeno-complex implantation (Control), xeno-complex implantation with rosiglitazone injection (RSG treatment), xeno-complex implantation with vehicle (Vehicle Control). After anesthetization, a 0.5–1 cm incision was made along the midline of the abdomen of the SD rat and xeno-complex were transplanted subcutaneously. RSG (Cayman Chemical, Ann Arbor, MI) was dissolved in dimethyl sulfoxide (DMSO) and then diluted in phosphate-buffered saline (PBS; pH 7.2) (1:3 solution). 10 μg of RSG (0.5 mg/mL) was locally administered at time points of 1 day, 2 days, and 3 days post-implantation using a 1-ml needle. During the post-surgery stages, all the SD rats were carefully kept by animal care technicians. The rats were euthanized and the implants were harvested at 3 days, 1 week, 3 weeks, 6 weeks, and 12 weeks. At the corresponding time points, tissue infiltration upon the xeno-complex was harvested for Taqman Gene expression assay immediately. The splenocytes were obtained by Ficoll density gradient centrifugation. All the implants were fixed in 4% neutral buffered paraformaldehyde and demineralized for at least 3 months. Thereafter, the tissues were embedded and sectioned into 5-μm-thick sections. Histological analysis and confocal immunofluorescence were applied for further evaluation.

2.4.2. TaqMan® gene expression assays

Total RNA was isolated from tissue infiltration upon xeno-complexes using the RNAiso plus Kit (TaKaRa Biotechnology, Dalian, China) according to the manufacturer's instructions. Synthesis of single-stranded cDNA from RNA was performed using a RevertAid First Strand cDNA Synthesis Kit (Thermo Scientific, USA) according to the manufacturer's instructions. Then, real-time PCR was carried out in quadruplicate for each gene using TaqMan Universal PCR Master Mix and TaqMan® Gene Expression assays (Thermo Scientific, formerly Applied Biosystems, Foster City, CA) on a QuantStudio™ 6 Flex Real-Time PCR System according to the manufacturer's instructions. The data were analyzed by DataAssist™ Software (Life Technologies™) and determined by the comparative CT method. GAPDH and Actb were used as the internal control genes. The ΔCt values were calculated by the global mean normalization strategy. P values were corrected for multiple testing using the Benjamini-Hochberg False Discovery Rate (FDR) method. The following TaqMan Gene Expression Assays (Thermo

Scientific, formerly Applied Biosystems, Foster City, CA) were used in the study: CD3e (Rn01422553_g1), CD4 (Rn00562286_m1), CD8A (Rn00580577_m1), FOXP3 (Rn01525092_m1), IL-1β (Rn00580432_m1), IFN-γ (Rn00594078_m1), TNF-α (Rn01525860_g1), IL-2 (Rn00587673_m1), IL-4 (Rn01456866_m1), IL-6 (Rn01410330_m1), IL-12 (Rn00575112_m1), TGF-β1 (Rn00572010_m1), IL-10 (Rn01483988_g1), PPARγ (Rn00440945_m1), FABP4 (Rn00670361_m1), STAT6 (Rn01505881_m1), CD68 (Rn01495634_g1), CCR7 (Rn02758813_s1), IRF5 (Rn01500522_m1), CXCL10 (Rn01413889_g1), VEGF (Rn01511602_m1), CD163 (Rn01492519_m1), MRC1 (Rn01487342_m1), ARG1 (Rn00691090_m1), CCL22 (Rn01536591_m1), PDGFA (Rn00709363_m1), MMP1 (Rn01486634_m1), MMP2 (Rn01538170_m1), MMP9 (Rn00579162_m1), TIMP1 (Rn01430873_g1), TIMP3 (Rn00441826_m1), Actb (Rn00667869_m1) and GAPDH (Rn01775763_g1).

2.4.3. Flow cytometry

The T lymphocyte subpopulations were analyzed by Flow cytometry as above described. Mouse anti-rat CD3-FITC, CD8-PE, Alexa Fluor® 488 anti-rat FOXP3, CD25-PE (Biolegend, USA), and CD4-PE-Cy5.5 (BD Biosciences) antibodies were used for measurement of $CD3^+CD4^+$, $CD3^+CD8^+$, and $CD4^+CD25^+FOXP3^+$ T cell percentages.

2.4.4. Confocal immunofluorescence

Xeno-complex with infiltrated tissues (3 days, 1 week, 3 weeks, 6 weeks, and 12 weeks) were fixed with 4% neutral buffered paraformaldehyde and demineralized for at least 4 months. Thereafter, the tissues were embedded and sectioned into 5-μm thick sections. The macrophage phenotypes in response to xeno-complex at intracavity or periphery sites were analyzed by confocal immunofluorescent labeling. Slides were deparaffinized and rehydrated, followed by antigen retrieval in heated citrate buffer for 20 min (10 mM citrate, pH 6.0, at 95–100 °C). For non-specific antibody binding, slides were blocked in a solution consisting of 2% normal horse serum (zsbio, Beijing, China), 1% bovine serum albumin (Sigma-Aldrich, St. Louis, MO, USA), 0.1% Triton X-100 (Sigma-Aldrich, St. Louis, MO, USA), and 0.1% Tween-20 (Sigma-Aldrich, St. Louis, MO, USA) in PBS for 1 h at room temperature. Sections were decanted and incubated with primary antibodies overnight at 4 °C. The following primary antibodies were used: the pan-macrophage marker, mouse anti-rat CD68 (Abcam, Cambridge, MA, UK), the M1 macrophage marker, rabbit anti-rat CCR7 (Abcam, Cambridge, MA, UK), and the M2 macrophage marker, goat anti-rat CD206 (Santa Cruz). Thereafter, sections were washed three times using PBS and incubated with secondary antibodies for 1 h at room temperature, including donkey anti-mouse-488 (Santa Cruz), chicken anti-rabbit-647, and donkey anti-goat-555. Then, after washing, the nuclei were labeled with DAPI, and the slides were coverslipped with a fluorescent mounting medium. Sections were imaged using the FV10i confocal biological inverted system (Olympus, Tokyo, Japan). The macrophage subsets were automatically quantified per field of view (40 × magnification) using CellProfiler software. 3–6 images were used for the statistical analysis of each group. Macrophages were defined as CD68 positive co-expressed with nuclei. M1 and M2 cells were counted as macrophages coexpressing CCR7 or CD206, respectively. The M2:M1 ratio was calculated as the (# of M2 macrophages +)/(# of M1 macrophages +).

2.5. Orthotopic implantation of xeno-complex in non-human primate

The experiment or specimens from Non-human primate (NHPs) were approved by the Research Ethics Committee of West China School of Stomatology and were conducted in WestChina-Frontier PharmaTech.

2.5.1. Non-human primate (NHPs)

Five adult male macaques, 5–6 years of age, 7–8 kg, were used for the present study. The macaques were looked after by animal care technicians, with regular sterile feeding of food, water, and fruits. The steel cages were cleaned in the morning every day. The mandibular central incisors and pre-molars were carefully extracted after anesthesia. When the sockets underwent healing for at least 3 months, xeno-complex were transplanted in situ in jaws using the implant unit after anesthesia. The surgery was performed under sterile conditions. The gingiva was closely sutured after surgery with periodontal pack treatment. Because of the difficulty application of the NHP model, two groups were divided into xeno-complex implantation (Control) and xeno-complex implantation with RSG injection (RSG treatment). The normal native tooth was used as a positive control (Native). RSG was locally administered into the chamber of xeno-complex at time points of 1 day, 2 days, and 3 days post-implantation using a 1-ml needle. As the precious source of NHPs, the surgery was performed in reverse order for short-term (1 week) and long-term (3 months) observation. Each NHP served as the 1-week group and 3-month group for the avoidance of individual differences. For each group, at least four implant sites were contained for statistical analysis. The macaques were euthanized after 3 months. Thereafter, the tissues that infiltrated upon xeno-complex at 1 week were harvested for gene assay of inflammatory cytokines, and the alveolar bone containing xeno-complex (1 week and 3 months) was sawed and fixed with 4% paraformaldehyde for Micro-CT scanning (Skyscan, Bruker) and histological analysis.

2.5.2. Real-time PCR

Total RNA was extracted from tissue infiltration upon xeno-complex in macaques. Then mRNA expression, such as macrophages-related factors and inflammation-associated cytokines, were analyzed according to the protocol described above. The expression levels for each gene were normalized to GAPDH (mean ± SEM; $n \geq 3$). The primer sequences are listed in Table S2.

2.5.3. Micro-CT scanning of the reconstructed tooth root in jaws of NHPs

Alveolar bone containing the xeno-complex was scanned by the SkyScan 1176 desktop X-ray Micro-CT System (Skyscan, Bruker). A high-resolution scan with an Image Pixel Size of 17.75 μm was recorded. The SkyScan 1176 system was operated by the energy of 90 kV and the intensity of 270 (μA), and the exposure time was set to 360 ms. Scanning was completed by 360 rotation around the vertical axis, with a rotation step of 0.500, using a 0.1 mm Cu filter. Then, two-dimensional (2-D) images and three-dimensional (3-D) images were obtained using the DateView and CT-Vox software (SkyScan, Bruker), respectively.

2.5.4. Three-dimensional finite element stress analysis

The biomechanical features of the reconstructed xeno-complex were analyzed based on the establishment of a three-dimensional finite element model using Mimics 16.0 (Materialise NV, Leuven, Belgium) and ANSYS Workbench 15.0 (ANSYS Inc., Canonsburg, PA, USA). Data collected from Micro-CT were imported into mimics 16.0, and a three-dimensional alveolar bone model containing xeno-complex and adjacent tooth was reconstructed through the threshold segmentation. After transportation of data into 3-Matic 8.0, the glass fiber post model was constructed according to the length of the pulp chamber of xeno-complex. The related parameters were showed as follows: upper length = 3 mm, lower length = the length of xeno-complex, and diameters at bottom = 0.5 mm, diameters at upper and cervical region = 0.9 mm. All these mentioned structural components were correlative with image masks for non-manifold assembly and were formatted to a three-dimensional presentation. Then these components were segmented using solid 10-node tetrahedral elements after importation into 3-Matic software. Thus, the volume mesh model was obtained, with different specimens showing similar nodes and similar elements. The refined mesh model was transformed back into Mimics. The material properties were submitted to the refined mesh based on

CT gray values of representative tissues, where red indicated higher density and larger elastic modulus, and blue indicated opposite properties. These refined meshes and material properties were obtained and exported into the required format for the establishment of a new finite element modeler in ANSYS Workbench15.0. Thereafter, the volume mesh model and the related material properties were visible when the edit mode was present. Force loading to mimic masticatory forces was applied to analyze the biomechanical features.

2.5.5. Histological analysis

All samples from macaques were demineralized for at least 3 months and embedded and sectioned into 5-μm-thick sections. Slides were deparaffinized and rehydrated for Hematoxylin and Eosin (H&E) staining or Masson's Trichrome staining according to the manufacturer's recommended protocol, thus observing the structural morphology of the regenerated root based on xeno-complex.

Immunohistochemistry was performed to evaluate the odontogenesis of the xeno-complex after xenotransplantation. Slides were deparaffinized and rehydrated through a graded ethanol series. After antigen retrieval, the slides were incubated for 1 h with goat serum working fluid at room temperature to prevent nonspecific antibody binding. Sections were decanted and incubated with primary antibodies overnight at 4 ˚C. Then, the slides were incubated with 3% hydrogen peroxide for 30 min at room temperature to inhibit endogenous peroxidase activity. After washing, the slides were incubated with the secondary antibody for 30 min at room temperature, followed by DAB staining. Images were obtained using a light microscope (Olympus BX43, Tokyo, Japan). The following primary antibodies were used: mouse anti-monkey/human DMP-1 and βIII-tubulin (Millipore, Billerica, MA, USA); rabbit anti-monkey/human periostin, COL-3 (Abcam, Cambridge, MA, UK); mouse anti-monkey/human COL-1 (Abcam, Cambridge, MA, UK); and mouse anti-monkey DSPP (Santa Cruz Biotechnology, Santa Cruz, CA, USA). CD31 was immunostained to verify blood vessel infiltration, which was then analyzed by confocal immunofluorescent labeling according to protocols in section 2.4.4. The primary antibodies were used: mouse anti-monkey/human CD31(Abcam, Cambridge, MA, UK).

2.6. Statistical analysis

The data are presented as the mean values ± SEM using GraphPad Prism (Graphpad Software, San Diego, CA, USA). One-way ANOVA and Tukey's multiple comparisons tests were applied for the statistical analysis of differences among more than two groups, while t-tests were used to analyze differences between two groups. All experiments were repeated multiple times (n ≥ 3). Differences between groups were considered significant when $*p < 0.05$, $\#p < 0.05$, $**p < 0.01$, $***p < 0.001$ and $****p < 0.0001$.

3. Results

3.1. Xenogeneic bioengineered tooth root complex (xeno-complex) triggered a Th1-type CTL response

We first sought to evaluate the cellular response to xenogeneic bioengineered tooth root complex (xeno-complex). Through by demineralization and decellularization, porcine-derived treated dentin matrix (pTDM) were fabricated. Then xeno-complex was constructed by seeding allogeneic dental follicle cells (aDFCs) onto pTDM for 7 days (Fig. 1A). The immunogenicity of xeno-complex (pTDM populated with human DFCs *in vitro*) or pTDM was both investigated via coculture with human peripheral mononuclear cells(hPBMCs) *in vitro* (Fig. 1B). After 5 days of coculture, both the pTDM and xeno-complex activated $CD3^+$ T lymphocytes in comparison to the hPBMCs control (Fig. 1C). The further sub-phenotypic analysis revealed that the majority of xeno-complex induced T cell proliferation was due to significant increased $CD3^+CD8^+$ T populations, indicating a cytotoxic T lymphocyte (CTL) response (Fig. 1C). No significant differences were detected between pTDM and xeno-complex induced $CD3^+$ T lymphocyte proliferation or between pTDM and xeno-complex induced $CD3^+CD8^+$ T lymphocyte proliferation. These findings suggested that xeno-complex induced CTL response was mainly caused by the immunologic properties of pTDM.

We then explored whether this CTL response interacted with T helper-1(Th1) or Th2 cytokines. Via tested by Luminex Multiplex MAP, cytokines released from the proliferated hPBMCs in all groups were showed in the heatmap (Fig. 1D), with red represented high concentrations vs. blue represented low concentrations. Compared with the hPBMCs control and the pTDM groups, a higher release of the pro-inflammatory cytokine Interferon-γ (IFN-γ) (8725 ± 1419 pg/ml, $p < 0.05$) was detected in the xeno-complex group. Accordingly, the xeno-complex group also released more interleukin-6 (IL-6) (7048 ± 154.9 pg/ml), with the statistical value of $p < 0.0001$ compared with the hPBMCs control, and $p < 0.001$ compared with the pTDM group. Besides, the xeno-complex group also had higher interleukin-12(IL-12) (13.87 ± 4.41 pg/ml) secretion than those of other groups($p < 0.05$). These pro-inflammatory cytokines, such as IFN-γ, IL-6, and IL-12, might contribute to an accompanied Th1 response. Whereas, there were no differences in interleukin-4(IL-4) concentrations between the groups, suggesting mere Th2 response.

3.2. PPARγ-primed macrophage polarization exhibited anti-inflammatory properties

To antagonize the induced CTL cellular response, the anti-inflammatory macrophage phenotypes were incubated (Fig. 2A). Ligand-activated peroxisome proliferator-activated receptor γ (PPARγ) not only masters the regulator of lipid metabolism, but also regulates inflammation and augment IL-4 primed M2 macrophage (M2a) polarization [17]. It was reported that macrophages lose the ability to suppress inflammation in the absence of PPARγ signaling [18]. This study applied PPARγ agonist, rosiglitazone (RSG), to promote a peripheral monocyte switch towards the alternative activated macrophage phenotype (M2γ) in the presence of IL-4. Both incubated M2γ and M2a phenotypes displayed specific cell processes in contrast to resting macrophages (M0) (Fig. S1A). Immunofluorescence assay then indicated elevated co-expression of CD68 and CD206 (M2 surface marker) in M2γ relative to M2a macrophages (Fig. S1B). Meanwhile, M2γ macrophages expressed a higher level of CD206 and FABP4 (a PPARγ target gene) and lower CCR7 (M1 surface marker) and STAT1(M1 activation) than that of M2a macrophages (Fig. S1C). All the data suggested an augment of the M2 macrophage phenotype of M2γ.

Then the properties of the M2γ phenotype were further evaluated. Flow cytometry analysis indicated that M2γ macrophages expressed more CD206 than that of M0 macrophages (Fig. 2B). Gene expression analysis (Fig. S2A) demonstrated that M2γ expressed significantly upregulated M2 markers CD206(approximately 10-fold higher than that of M0) and AMAC-1(Alternative macrophage activation-associated CC chemokine 1). Respectively, upregulated TGF-β1 and IL-10 as well as downregulated IL-1β and TNF-α in M2γ macrophages confirmed its capacities to mediate inflammation. The higher expression of TIMP1, TIMP3, and the lower expression of MMP1, MMP2, MMP9 suggested pro-fibrotic features for M2γ macrophages. Additionally, increased levels of vascular endothelial growth factor (VEGF) and platelet-derived growth factor (PDGF) further verified the ability of M2γ to promote angiogenesis. The M2γ supernatants, termed as M2γ medium, were collected and tested by Luminex. High release of IL-4 and lower secretion of IL-6, IL-8, tumor necrosis factor-α (TNF-α) indeed revealed the anti-inflammatory capacities of M2γ medium (Fig. 2C). Collectively, PPARγ-primed macrophage polarization exhibited pro-wound-healing, anti-inflammatory, pro-fibrotic, and tissue-regenerating properties.

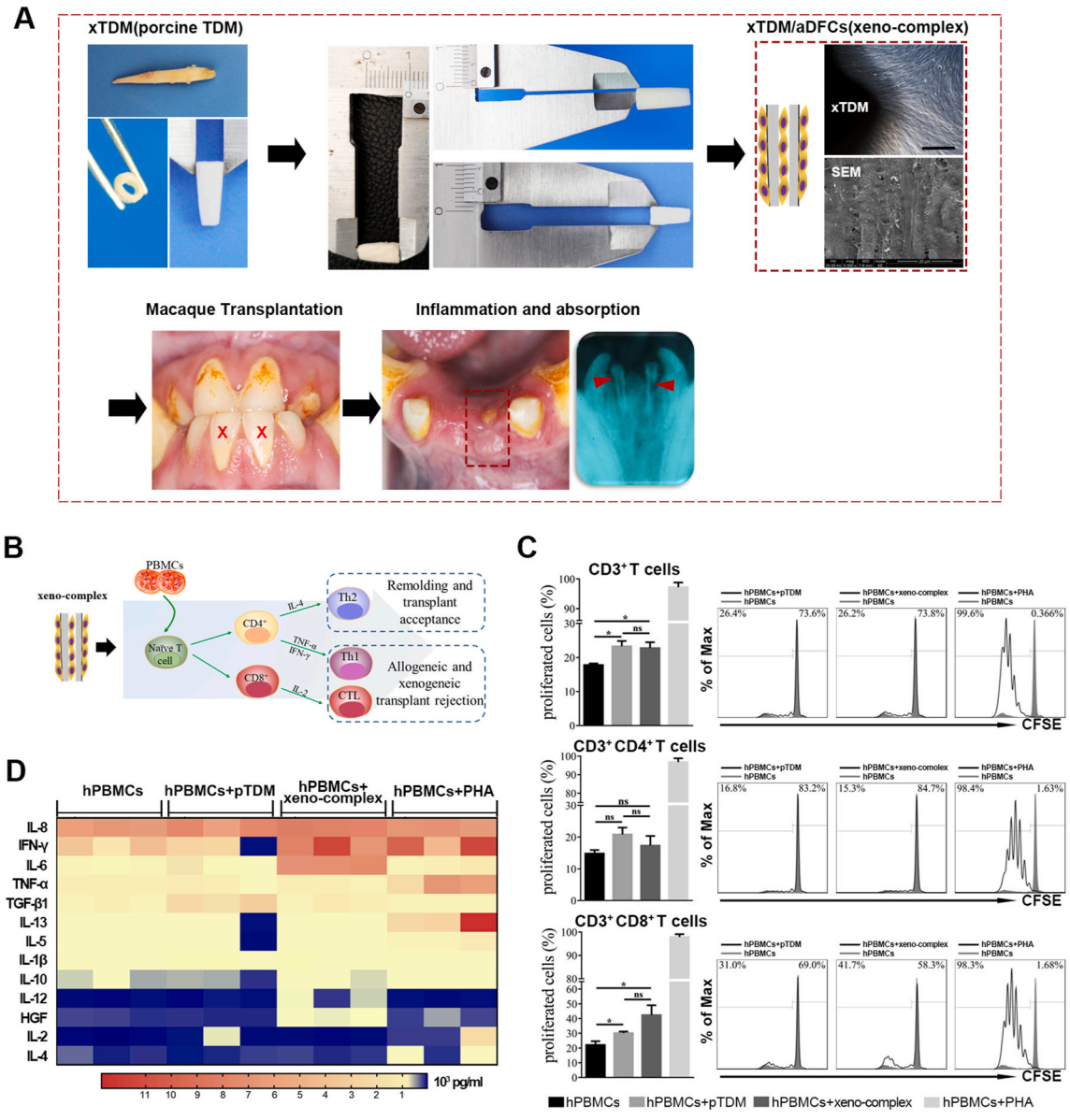

Fig. 1. Xenogeneic bioengineered tooth root complex(xeno-complex) triggered a Th1-type $CD3^+CD8^+$(CTL) cellular response. (A) Bioactive xeno-complex were transplanted in macaque orthotopically, and inflammation and absorption were observed. (B)The schematic diagram to evaluate cellular response to xeno-complex *in vitro*. (C) Flow cytometry analysis (FACS) was performed on a CFSE-based lymphocyte proliferation in response to pTDM or xeno-complex, with a suboptimal dose of anti-CD3 stimulus at 0.025 μg/ml. The proliferated $CD3^+$, $CD3^+CD4^+$, and $CD3^+CD8^+$ lymphocytes were graphed as an overlay (black line) in each FACS histogram covering CFSE-stained hPBMCs (gray shaded histogram). hPBMCs without stimulus was the negative group, and Phytohemagglutinin (PHA) stimulation was the positive group. The % value on the left defined the level of proliferated immune cells within 5 days. Data are means ± SEM (n ≥ 3). *$p < 0.05$. (D) Th1/Th2 cytokines released from hPBMCS in response to pTDM or xeno-complex were analyzed using Immunology Luminex® Multiplex MAP. The heatmap was presented such that red indicated high concentrations vs. blue represented low concentrations (pg/ml). (For interpretation of the references to colour in this figure legend, the reader is referred to the Web version of this article.)

3.3. M2γ macrophages suppressed Th1-type CTL response that triggered by xeno-complex

We further explored whether these activated macrophage phenotypes regulate cellular response induced by xenogeneic bioengineered organs. To test this, the M2γ medium was incubated in the coculture system of xeno-complex with hPBMCs *in vitro* (Fig. S2B). Respectively, both the proliferated $CD3^+$ T and $CD3^+CD8^+$ CTL lymphocytes, stimulated by xeno-complex, were significantly reduced by the M2γ medium (Fig. 2D). Parallelly, incubation with M2γ medium also resulted in downregulated TNF-α expression of hPBMCs in the xeno-complex group (Fig. 2E). Thus, M2 macrophages exert paracrine anti-inflammatory effects not only on M1 macrophages but also on cellular response induced by xeno-complex.

PPARγ activation could exert anti-inflammatory effects via trans-repression of inflammation-associated target genes [19]. We then sought to evaluate whether PPARγ activation alone mediates cellular response induced by xeno-complex, with the absence of IL-4. As expected, RSG treatment inhibited proliferated $CD3^+CD8^+$ CTL cells triggered by xeno-complex (Fig. 2D), accompanied by an inhibition of TNF-α and IFNγ expression (Fig. 2E). Previous reports showed that PPARγ activation *in vitro* only modulates M2 markers in monocytes polarized to M2 in the presence of IL-4 and/or IL-13 [17]. However, via immunofluorescence stains of macrophages in all coculture groups

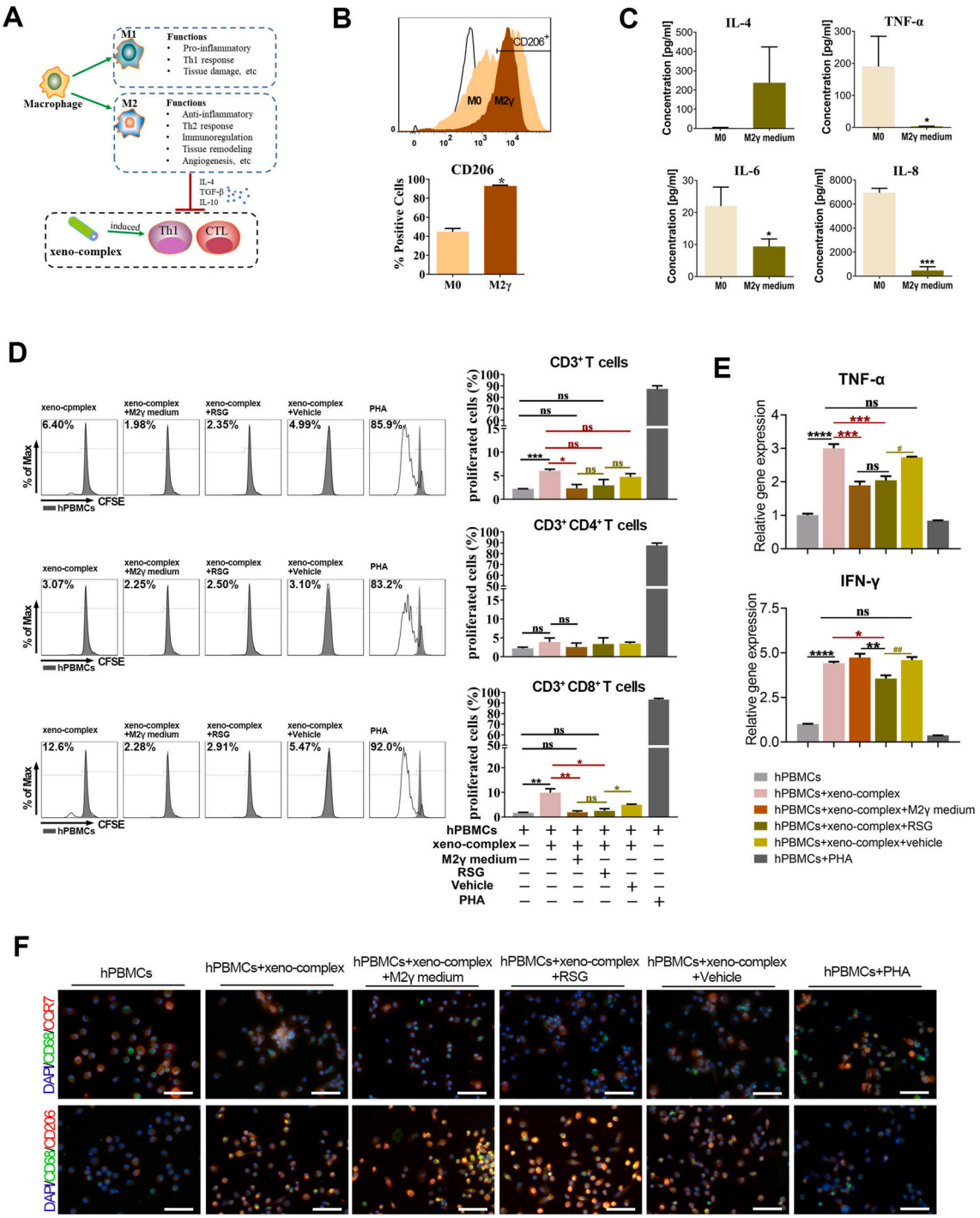

Fig. 2. M2γ macrophages suppressed the Th1-type CTL response triggered by xeno-complex *in vitro*. (A) The hypothesis that polarized M2 macrophages perform anti-inflammatory effects on cellular response triggered by xeno-complex. (B) Incubation and identification of PPARγ-primed macrophages (M2γ). Human peripheral monocytes were primed towards M2γ macrophages via the addition of rosiglitazone (RSG) in the presence of IL-4. The M2γ macrophages were obtained after incubation for 7 days. The phenotype marker CD206 was identified by Flow cytometry analysis (FACS). Data are means ± SEM (n ≥ 3). $*p < 0.05$. (C) Identification of M2γ conditional medium (M2γ medium). The anti-inflammatory and pro-inflammatory cytokines were analyzed using Immunology Multiplex MAP. Data are means ± SEM (n ≥ 3). $*p < 0.05$, $***p < 0.001$. (D) M2γ medium or RSG inhibited proliferated $CD3^+CD8^+$ cells triggered by xeno-complex. The cellular response to xeno-complex was quantified by FCS using CFSE-based proliferation assay. The proliferated $CD3^+$, $CD3^+CD4^+$, and $CD3^+CD8^+$ lymphocytes were graphed as an overlay (black line) in each FACS histogram covering hPBMCs (gray shaded histogram). hPBMCs without stimulus was the negative group, and PHA stimulation was the positive group. The % value on the left defined the level of proliferated cells within 5 days. Data are means ± SEM (n ≥ 3). $*p < 0.05$, $**p < 0.01$. (E) hPBMCs in the six coculture systems were measured for mRNA expression of pro-inflammatory TNF-α, INF-γ. The data were normalized to those of GAPDH mRNA and are presented relative to those of hPBMCs without any stimulus, set as 1. Data are means ± SEM (n ≥ 3). $*p < 0.05$, $**p < 0.01$, $***p < 0.001$, $****p < 0.0001$; NS, no significance. (F) The adherent monocytes/macrophages differentiation in the six coculture systems were co-immunostained with antibodies against CD68/CCR7 or CD68/CD206, DAPI was used for nuclear staining. Scale bars, 50 μm.

(Fig. 2F), the positive coexpression of $CD68^+CD206^+$ M2 macrophages in RSG treatment groups were in line with M2γ medium groups, more than those of other groups. PPARγ activation might promote M2 polarization in a cocultured immune-environment without IL-4 addition, such as slight IL-4 released from PBMCs. As a result, PPARγ activation could directly suppress cellular response induced by xeno-complex via M2 polarization.

3.4. PPARγ activation inhibited cellular response to xeno-complex via promoting M2 polarization in vivo

To determine whether these observations also occur *in vivo*, the cellular response to xeno-complex were sequentially investigated, with RSG treatment or not, after xenotransplantation (Fig. 3A). Here, xeno-complex were constructed by populating pTDM with allogeneic rat

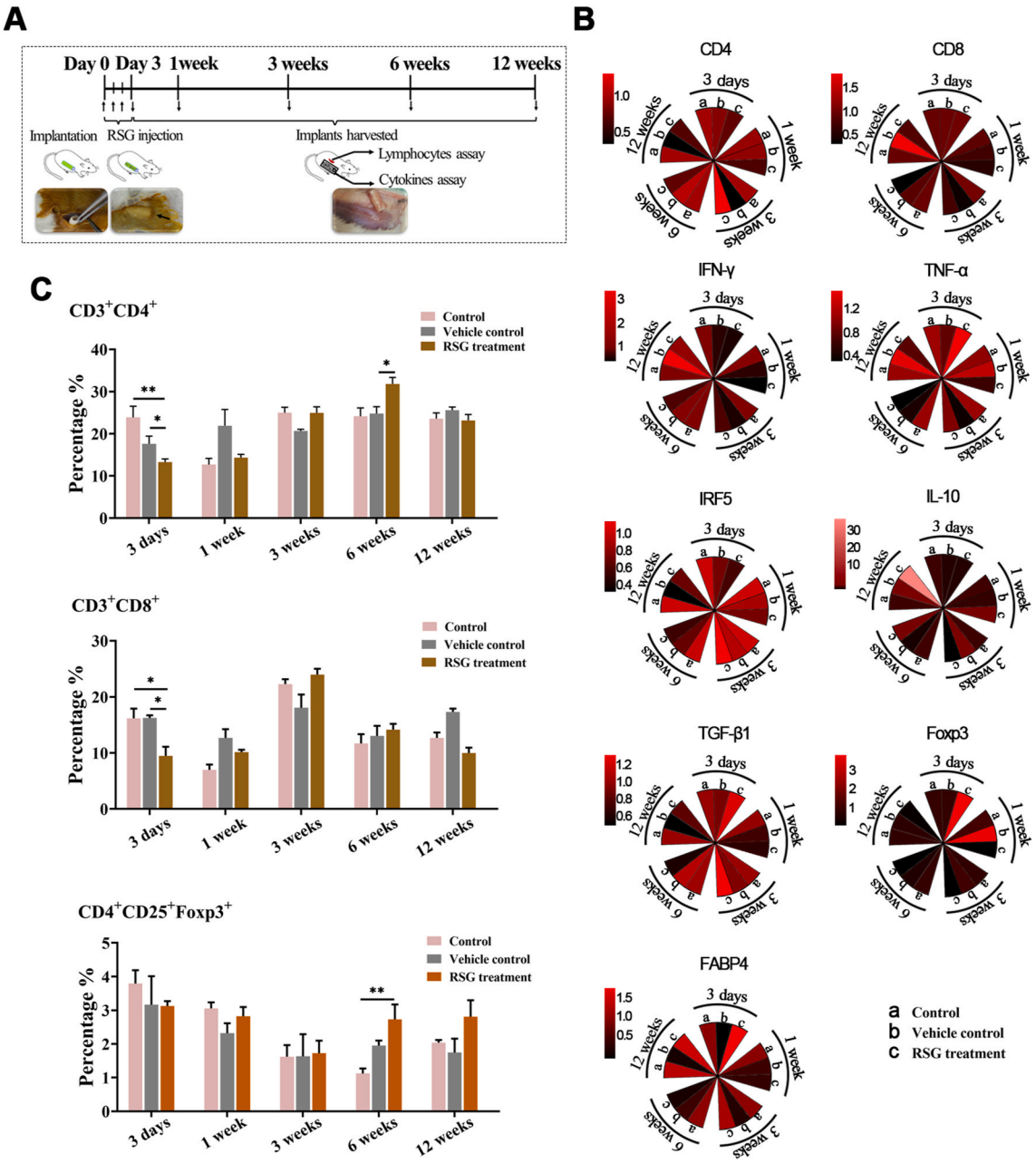

Fig. 3. PPARγ activation inhibited host cellular response to xeno-complex *in vivo*. (A) The schematic diagram of sequential investigation on host response to xeno-complex *in vivo*. Xeno-complex were constructed by populating pTDM with allogeneic rat derived DFCs(rDFCs), and were subcutaneously transplanted in rats. RSG was locally administered postoperative 1–3 days. Xeno-complex with no treatment (Control) or with vehicle (Vehicle control) served as controls. Implants were harvested at postoperative 3 days, 1 week, 3 weeks, 6 weeks, and 12 weeks, and the host response was analyzed at the local implantation site (cytokines assays) and in the periphery system (lymphocytes assays). (B) RNA from tissues infiltrating upon xeno-complex were isolated and measured by Taqman gene expression assays. The inflammation-associated cytokines were sequentially evaluated. Each result was normalized to those of GAPDH mRNA and are presented relative to those of Control at 3 days, set as 1. The heatmap was presented such that red indicated higher values vs. black represented lower values. (C) Splenic lymphocytes were isolated and assayed using FACS analysis, including $CD3^+CD4^+$, $CD3^+CD8^+$, and $CD4^+CD25^+$ $Foxp3^+$ T cells. Data are mean ± SEM (n ≥ 3), $^*p < 0.05$, $^{**}p < 0.01$. (For interpretation of the references to colour in this figure legend, the reader is referred to the Web version of this article.)

derived DFCs(rDFCs), and were subcutaneously transplanted in rats after 7 days incubation. Inflammation-associated cytokines and macrophage-mediated factors were sequentially measured in RNA isolated from tissues infiltrating upon xeno-complex (Fig. S3B). RSG was injected locally at the beginning 3 days, and elevated expression of FABP4 (PPARγ targeted gene) was detected at 3 days (Fig. 3B). As expected, PPARγ activation resulted in a decreased CD4 expression at 3 days and 1 week, as well as reduced CD8 levels at 1 week (Fig. 3B). Parallelly, the pro-inflammatory molecules, such as IFN-γ and Interferon regulatory factor 5(IRF5), were inhibited by RSG treatment both at 3 days and at 1week. Whereas, TNF-α displayed a delayed reduction at 1week in line with CD8 expression in the RSG treatment group. Concerning anti-inflammatory factors, PPARγ activation contributed to a prolonged increase of TGF-β1 and Foxp3 at 3 days as well as IL-10 at 1 week (Fig. 3B). Collectively, the acute tissue response to xeno-complex was immunosuppressed by PPARγ activation.

Meanwhile, a systemic response was measured. In line with local response, both splenic $CD3^+CD4^+$ T and $CD3^+CD8^+$ T lymphocytes at 3 days were reduced by RSG treatment (Fig. 3C, Fig. S4A, and Fig. S4B). Interestingly, an arise of $CD3^+CD4^+$ T lymphocytes was detected at 6 weeks in the RSG treatment group. This phenomenon might be attributed to the elevated $CD4^+CD25^+Foxp3^+$ T cells (Fig. 3C and Fig. S4C), which generally govern immune-regulating effects. Therefore, these inhibitory responses exerted by PPARγ activation were mainly presented at the early phase, with no adverse effects on long-time observations.

We next asked whether these effects of PPARγ activation were associated with macrophage polarization. The infiltrated macrophages were semi-quantified sequentially, either at the intracavity or periphery of the transplanted xeno-complex (Fig. 4). RSG treatment statistically provoked M2 polarization ($CD68^+CD206^+$) from 1 week to 3 weeks at the periphery sites (Fig. S5A), whereas 3 days to 1 week at intracavity sites (Fig. S5B). Meanwhile, relatively low numbers of M1 phenotype ($CD68^+CCR7^+$) were detected from 3 days to 6 weeks at both the two sites with RSG treatment (Fig. S5). For precise analysis, the percent ratio of M2 cells to M1 cells (M2/M1 ratio) was also calculated (Fig. 4). At both intracavity and periphery sites, RSG treatment resulted in a ratio of M2/M1 ≥ 1 from 3 days until 12 weeks, while other groups display M2/M1 ≥ 1 from 6 weeks (Fig. 4D). And there was no statistical difference in M2/M1 radios among the three groups at 12 weeks. RSG treatment mainly modulated macrophage polarization at the early phase, in line with those inhibitory effects on cellular response. Taken together, PPARγ-primed $CD68^+CD206^+$macrophage effectively inhibited acute cellular response initiated by xenotransplantation of bioengineered organs.

3.5. PPARγ-primed macrophage inhibited acute inflammation after orthotopic implantation of xeno-complex in nonhuman primates

To confirm whether these findings could be translated to nonhuman primates, xeno-complexes were orthotopically implanted into a healed alveolar socket of macaques. Here, pTDM seeded with allogeneic mDFCs (monkey-derived DFCs) were incubated as xeno-complex (Fig. 5A). RSG treatment significantly increased M2 marker CD206 after 1week implantation of xeno-complexes, accompanied by lower expression of MMP1, MMP2, and MMP9 (Fig. 5B). Correspondingly, the pro-inflammatory cytokines IL-1β, TNF-α, IL-6, and AP-1 were significantly downregulated in RSG treatment group (Fig. 5C). Elevated expression of the Th2-associated cytokine IL-4 was observed with RSG treatment (Fig. 5C), which further verified the anti-inflammatory capacities of PPARγ-primed macrophage.

Since the seasonable-controlled of cellular response by PPARγ-primed macrophage, well-arranged connective tissues were evident at both intracavity (Fig. 5D) and periphery (Fig. 5E) sites of xeno-complex. In contrast, the control groups initiated disorganized tissues in the intracavity (Fig. 5D), and a few fibroblasts were distributed between the xeno-complex and alveolar bone (Fig. 5E). Taken together, PPARγ-primed macrophage significantly suppressed xeno-complex-induced acute inflammation and initiated the tissue repair process at 1week post-implantation in non-human primates. Then, CD31 was immunostained to verify blood vessel infiltration. Abundant $CD31^+$ endothelial cells were recruited and distributed at 1week post-implantation of xeno-complexes without RSG treatment (the control group), both at the intracavity and periphery sites (Fig. 5F). While the numbers of $CD31^+$ endothelial cells were decreased in contrast to the control group, and the $CD31^+$ cells likely trended to fusion in the RSG treatment group (Fig. 5F). The recruited endothelial cells prompt angiogenesis via a process of sprouting, anastomosis, and maturation [20]. This result was in line with the kinetics interplay of macrophage-endothelial cells in angiogenesis, that M1 macrophages promote sprouting of endothelial cells while M2a promotes the fusion of blood vessels at a later phase [21].

3.6. PPARγ-primed macrophage enabled xeno-complexes to regenerate morphology-biomechanical equivalency to native roots

Since host-graft cellular responses were significantly inhibited by PPARγ-primed macrophage, we sought to explore whether an architecture-morphological equivalency to normal tissue would be re-established. Until three months post-implantation, RSG treatment facilitated favorable integrity of xeno-complexes with the alveolar bone, while aberrant absorption in the control group was observed (Fig. 6A). A new static structural modeler was set up in ANSYS Workbench15.0 to evaluate the biomechanical properties of xeno-complexes in alveolar bone [22]. An oblique push of 111.8 N was imposed to mimic masticatory force (Fig. 6B). No points of stress concentration were detected in the whole model. Consistent with the physical vibration/mobility of normal teeth, a total deformation (TD) of 0.3 mm was clustered at the crown cusp of the native tooth, verifying the reliability of force loading (Fig. 6B, ii). With these parameters, xeno-complexes, treated with RSG (0.035 mm) or not(0.02 mm), showed close TD values to native tooth roots (0.03 mm), indicating a mere loosening of the xeno-complexes. Equivalent von-mises stress (EQV) of the analyzed xeno-complex model mainly concentrated on the post, in line with the conditions in the natural post-restored tooth. The reconstructed root of xeno-complexes, treated with RSG or not, displayed EQV values approximate to native tooth roots, contributing to supporting for masticatory forces.

Even though there was no difference in the biomechanical properties between the control and RSG treatment groups, the aberrant absorption in control groups led to pathological fibrosis both at intracavity and periphery of xeno-complexes. As expected, H&E and Masson staining in the RSG treatment group revealed cells assembled at the inner border of the regenerated dentin (rD), contributing to morphological odontoblast-like cells (OdL) formation (Fig. 6C). The pulp-dentin complex was reconstructed, exhibiting native pulp tissue-like structures such as blood vessels, fibroblasts, and well-arranged collagen fibers (Fig. 6C). When concerned about periodontal tissue reconstruction, although newly formed blood vessels and collagen fibers were observed in the control group, the widen tissues, as well as mono-directional collagen fibers parallel to xeno-complex surface, were merely responsible for bearing occlusal forces (Fig. 6D). While in the RSG treatment group, a few cells in lacunas located at the outer margins of xeno-complex were observed, like cementocytes observed in the native cementum (Fig. 6D, yellow arrows), resulting in regenerated cementum (rC). And the pink-stained (H&E) or blue-stained (Masson) collagen fibrils connected the xeno-complex with alveolar bone in multiple orientations, even inserting into the regenerated cementum and alveolar bone (Fig. 6D). Nourished by newly formed vessels, these oriented collagen fibrils contributed to the formation of regenerated periodontal ligaments(rPDLs) like native PDLs, which would be responsible for the dissipation of occlusal forces. These well-organized rC, rPDLs, and alveolar bone made up the integrity of the cementum-PDLs-

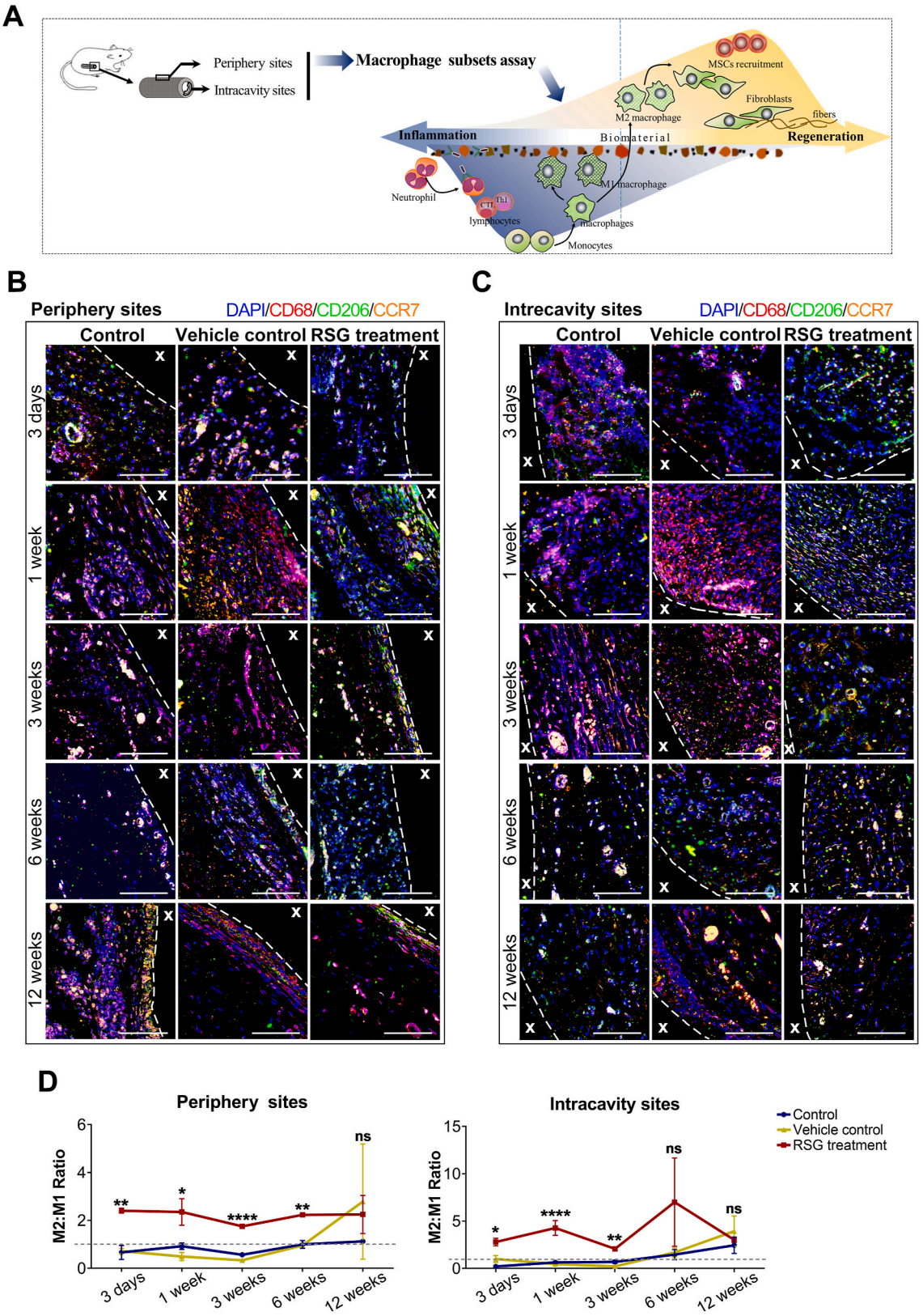

Fig. 4. PPARγ activation locally modulated M1-to-M2 tissue macrophage polarization. (A) The schematic diagram illustrated the correlation between M1/M2 macrophage phenotypes and the fate of implanted ECM. Macrophage polarization in response to xeno-complex were sequentially observation at postoperative 3 days, 1 week, 3 weeks, 6 weeks, and 12 weeks. Xeno-complex with RSG treatment served as experimental groups, while with no treatment (Control) or with vehicle (Vehicle control) served as controls. Macrophage phenotypes (B) at periphery sites and (C) in the intracavity sites of xeno-complex were shown by representative confocal immunofluorescence images. Co-immunostaining of pan-macrophage cell surface marker CD68 (red), the M1 marker CCR7 (orange), and the M2 marker CD206 (green) were merged with nuclear staining DAPI (blue). Scale bars, 50 μm. (D) A ratio was calculated as to the percentage of M2 cells to M1 cells (M2/M1 radio). The gray dotted line represented M2/M1 radio as 1.0, with over 1.0 indicating predominant M2 vs. below 1.0 representing predominant M1 cells. Data are mean ± SEM (n ≥ 3), $^{*}p < 0.05$, $^{**}p < 0.01$, $^{****}p < 0.0001$. NS, no significance. (For interpretation of the references to colour in this figure legend, the reader is referred to the Web version of this article.)

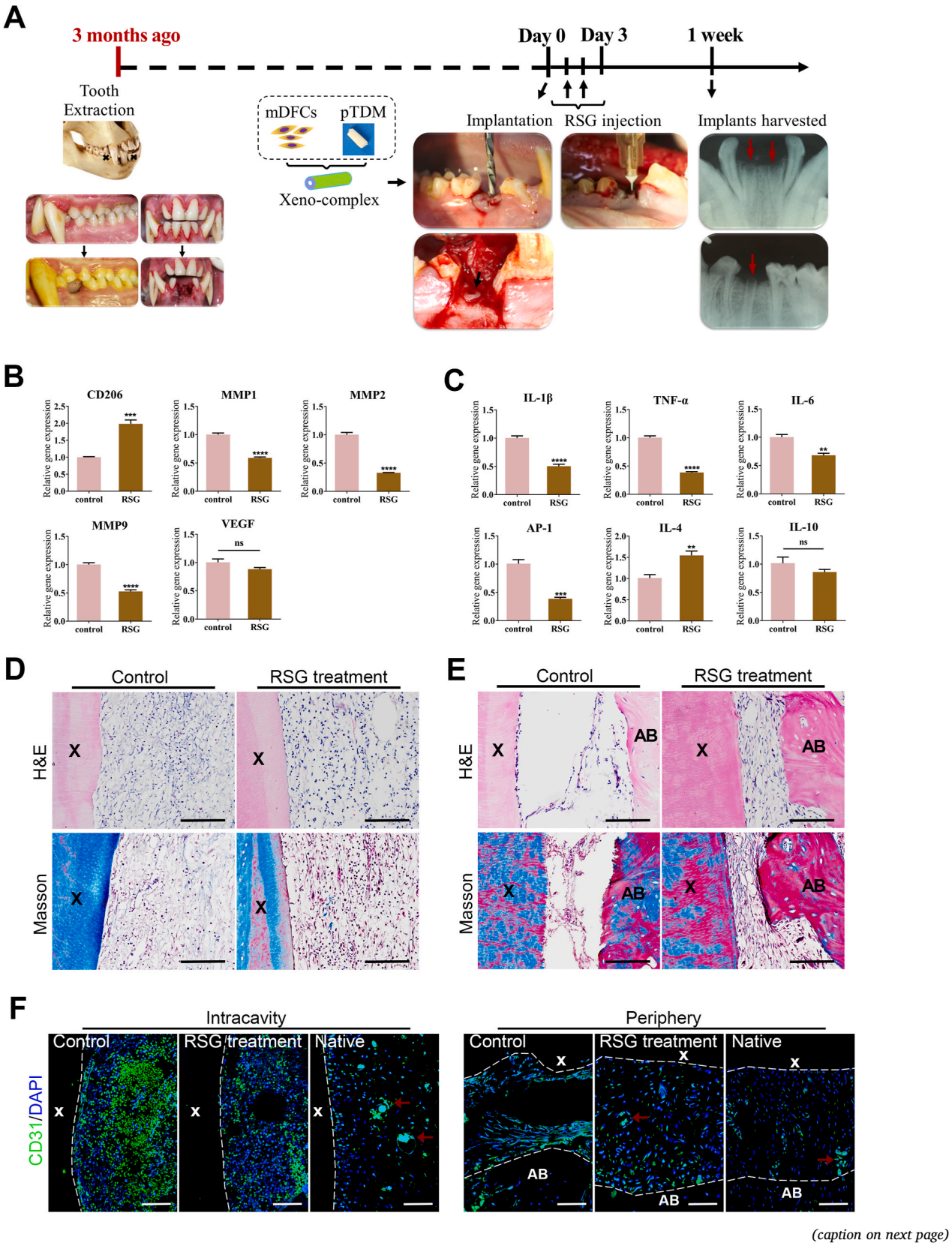

(caption on next page)

Fig. 5. PPARγ-primed macrophage inhibited acute inflammation after orthotopic implantation of xeno-complex in Non-human primates. (A) The schematic diagram illustrated the orthotopic implantation of xeno-complex in macaques. The dentition defect model was established in the jaws of macaques. After the extraction sockets underwent healing for at least 3 months, xeno-complex were randomly implanted into the dentition defects. RSG was locally administered at postoperative 1–3 days. Xeno-complex with no treatment served as Control. Implants along with alveolar bone were retrieved at 1week post-implantation for acute inflammation evaluation. Tissues infiltrating upon xeno-complex were analyzed for mRNA expression of (B) macrophages associated markers (CD206, MMP1, MMP2, MMP9, VEGF) and (C) Th1/Th2-associated cytokines (IL-1β, TNF-α, IL-6, AP-1, IL-4, IL-10). All data are normalized to those of GAPDH mRNA and are presented relative to those of Control, set as 1. All data are mean ± SEM (n ≥ 3), $^{**}p < 0.01$, $^{***}p < 0.001$, $^{****}p < 0.0001$. NS, no significance. (D) H&E staining and Masson staining of tissues at the intracavity of xeno-complex. Scale bars, 100 μm. (E) H&E staining and Masson staining of tissues at the periphery of xeno-complex. Scale bars, 100 μm. (F) Confocal immunofluorescent labeling showed $CD31^+$ endothelial cells in the control, the RSG treatment group, and the native roots. Red arrows: blood vessels. Scale bars, 100 μm. (X: xeno-complex, AB: alveolar bone). (For interpretation of the references to colour in this figure legend, the reader is referred to the Web version of this article.)

bone complex. Therefore, PPARγ-primed macrophage enabled xeno-complex to finally process as a regenerated tooth root, which behaved morphology-biomechanical equivalency to native roots.

3.7. PPARγ-primed macrophage facilitated functional xenogeneic tooth root regeneration

To determine whether the xenogeneic microenvironment and inflammation affected the odontogenesis of the xeno-complexes in non-human primates, odontogenesis-related proteins were evaluated by immunohistochemistry. All dentin, from early (1 week) to late phase (3 months), were positively stained of dentin matrix protein-1 (DMP1), indicating the bioactivity and remineralization of xeno-complexes [23] (Fig. S6A and Fig. 7A). As for tissues in the pulp chamber, the major ECM components marker (Col-I) and neuronal marker (β-tubulin III) were consistently expressed during all phases, with RSG treatment or not (Fig. S6A and Fig. 7A). Whereas, odontoblast-related markers, such as DSPP (Dentin sialophosphoprotein) and periostin, were merely expressed without RSG treatment both at the early phase (Fig. S6A) and late phase (Fig. 7A). The effective staining of DSPP in the odontoblast-like cell (OdL) and periostin in the subodontoblast layer confirming morphological and functional features of a regenerated pulp-dentin complex in the RSG treatment group.

When concerned about the periodontal tissues, positive expression of col-I (all phases) and col-III (merely expressed at early phase) were detected in the two groups (Fig. S6B and Fig. 7B). Although the involvement of col-I and col-III stated fibrogenesis, the morphological differences indicated pathological fibrosis in control group while functional features of rPDLs in RSG treatment group. Neuronal marker (β-tubulin III) was consistently positively stained in the two groups in line with tissues in pulp chamber. In contrast to slight expression in Controls, both consistently expressed DSPP and periostin were detected in RSG treatment group during all phases(Fig. S6B and Fig. 7B), which were essential to the integrity and function of rPDLs [24]. Taken together, PPARγ-primed macrophage effectively controlled the host-to-graft cellular response and facilitate functional xenogeneic tooth root regeneration.

4. Discussion

This study applied xenogeneic bioengineered tooth root regeneration to serve as a specific model to study the integrity of parenchymal and stromal tissue regeneration based on xenogeneic extracellular matrix (ECM). Treated dentin matrix (TDM) has been identified as an ideal scaffold for induced odontogenesis [15,25]. Bioactive materials and suitable seeding cells are crucial for tooth root regeneration [26]. In the former, porcine TDM (pTDM) could act as a promising alternative to solve the limited source of human TDM. pTDM exhibited similar characteristics to human dentin, such as the microstructure of hydroxyapatite crystals, the corresponding binding-energy, the remained functional groups and the similar mineral-to-collagen ratio [14]. In the latter, ideal seeding cells should be capable of differentiating into two types of cells to form both the pulp-dentin complex and the PDL/cementum-like tissue. Dental papilla cells and dental pulp cells have been thought to be the best seeding cells for dentin regeneration [27], yet are limited to introducing periodontal tissue regeneration. DFCs are the precursor cells of periodontal tissues, and could generally differentiate into cementoblasts, periodontal ligament cells, and alveolar bone cells [28]. Moreover, we previously found that pTDM could act as essential substrates to induce human DFCs (hDFCs) to undergo odontogenic differentiation [14]. Therefore, a pTDM-based scaffold populated with allogeneic DFCs (aDFCs) was utilized for tooth root regeneration. The present study further explored promising strategies to orchestrate the graft immune tolerance. We identified PPARγ-primed macrophage as an effective target to inhibit xenogeneic host-graft cellular response, such as Th1-type CTL response, *in vitro*, and *in vivo*. When translated to an orthotopic nonhuman primate model, PPARγ-primed macrophage significantly facilitated xenogeneic tooth root regeneration (i) by immunosuppressing IL-1β, IL-6, TNF-α, AP-1, MMPs to enable xenogeneic implants effectively escape an immune-mediated rejection and rescue an outcome of pathological fibrosis (ii) with morphology-biomechanical equivalency to a native tooth root, such as odontoblast-like cells in the pulp-dentin complex as well as cementocytes and oriented collagen fibrils in the cementum-PDLs-bone complex (iii) by rescuing partially injured odontogenesis such as DSPP and periostin expression.

Our findings firstly unveiled a Th1-type $CD3^+CD8^+$ cellular response induced by porcine TDM, opposite to the traditionally reported biocompatibility of ECM [29]. The ECM is initially proposed to be immune-privileged since the native source. However, some clinical outcomes of dense fibrous warn that the ECM components might also trigger a foreign body response until completely absorbed or cleared [6,30]. Evidence proposes that porcine col-I, the primary class of ECM, *in vitro* induces human $CD3^+CD8^+$ T cell proliferation accompanied by a strong release of the Th1-derived cytokines IFN-γ and TNF-α [16]. These scenarios also occur in porcine TDM in our experiment. TDM undergo demineralization and subsequently release the major molecules to mediate neighboring odontogenesis, such as col-I, DMP1, and DSPP [15]. The proteins-induced cellular response colluded with matrix metalloproteinases (MMPs), which in return degraded these proteins [31,32] and resulted in aberrant absorptions of xeno-complex in primates' model. Yet, serious adverse reactions are little reported even though fibrosis outcomes of xenogeneic ECM products in humans. This perhaps due to the traditional ECM performance that undergoes degradation and releases biologic components for native tissue remodeling [2]. The mechanical strength of these ECM-based tissue remodeling would be in a dynamic state, from a short-time diminishment to the newly matrix deposition [33]. Thus, the most commonly xenogeneic ECMs are applied for soft/stromal tissue remodeling. Nonetheless, the degradation process and cellular response are undesirable for the integrity of parenchymal and stromal tissues regeneration, since ECM here itself also support as structure-biomechanical stability for host cells to infiltrate, like TDM [22] and bone ECM. This requirement remains a daunting challenge.

Cumulative evidence have confirmed a close correlation between macrophage phenotype and the fate of implanted ECM [11,21]. Macrophages are verified not only as phagocytic and antigen-presenting cells, which mainly lead to biomaterial encapsulation and failure. The nomenclature M1, M2 phenotypes, and even disputable foreign body

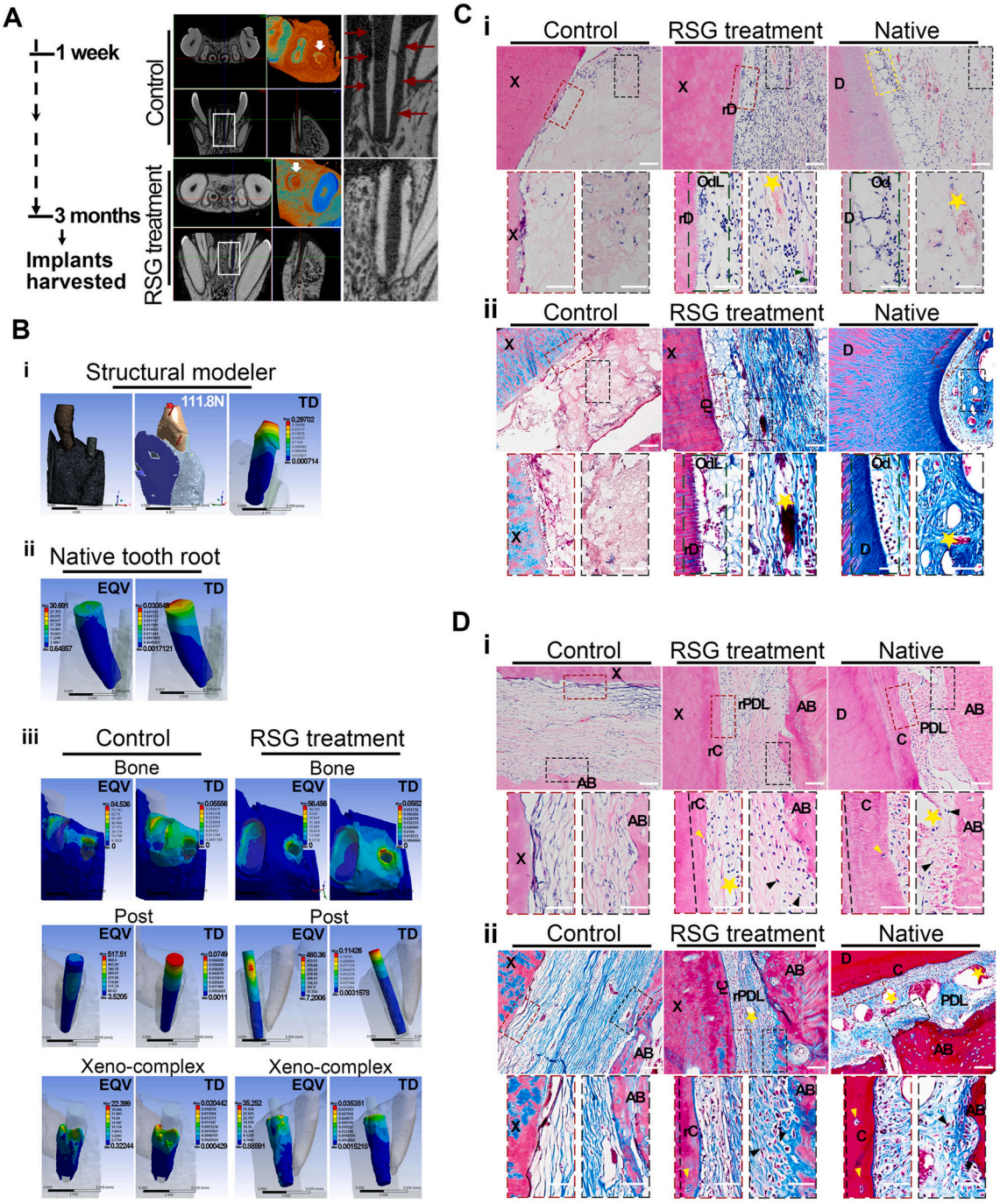

Fig. 6. PPARγ-primed macrophage enabled xeno-complexes to regenerate morphology-biomechanical equivalency to native roots (A) Until three months post-implantation, xeno-complex along with alveolar bone were harvested for morphology-biomechanical assay. The three-dimensional structure of xeno-complexes was presented by Micro-CT scanning. Red arrows showed aberrant absorption in the control group. (B) Biomechanical properties of xeno-complex in alveolar bone were analyzed using ANSYS Workbench. (i) a static structural modeler was set up, and an oblique push of 111.8 N was imposed to mimic masticatory force; (ii) Equivalent von-mises stress (EQV) and total deformation (TD) of native tooth root; (iii) EQV and TD of adjacent alveolar bone, post and xeno-complex in control and RSG treatment groups. (C) A pulp-dentin complex-like tissue was formed in the RSG treatment group, in line with that of native, by (i) H&E and (ii) Masson staining. X: xeno-complex; rD: regenerated dentin; OdL: odontoblast-like cells; D: dentin; Od: odontoblast. Green arrows: fibroblasts; Yellow stars: blood vessels. Scale bars, 100 μm(above) and 50 μm(below). (D) A cementum-PDLs-bone complex-like tissue was formed in the RSG treatment group, in line with that of native, by (i) H&E and (ii) Masson staining. X: xeno-complex; D: dentin; rC: regenerated cementum; rPDL: regenerated PDLs; AB: alveolar bone; Yellow arrows: cementocytes-like cells; Black arrows: oriented collagen fibrils and fibroblasts; Yellow stars: blood vessels. Scale bars, 100 μm(above) and 50 μm(below). (For interpretation of the references to colour in this figure legend, the reader is referred to the Web version of this article.)

giant cells (FBGC) are also involved in the integrity of non-degradable ECM and the replacement of degradable ECM [34,35]. Most studies described " macrophage polarization to modified ECM ″ as only conclusive statements [36]. This study recruited M2 polarization and thus creating a favorable immuno-microenvironment to initiate xenogeneic ECM-based tissue regeneration including (i) orchestrating graft immune tolerance and (ii) promoting odontogenesis with compositional parenchymal and stromal tissues. In the former, tissue injuries and host

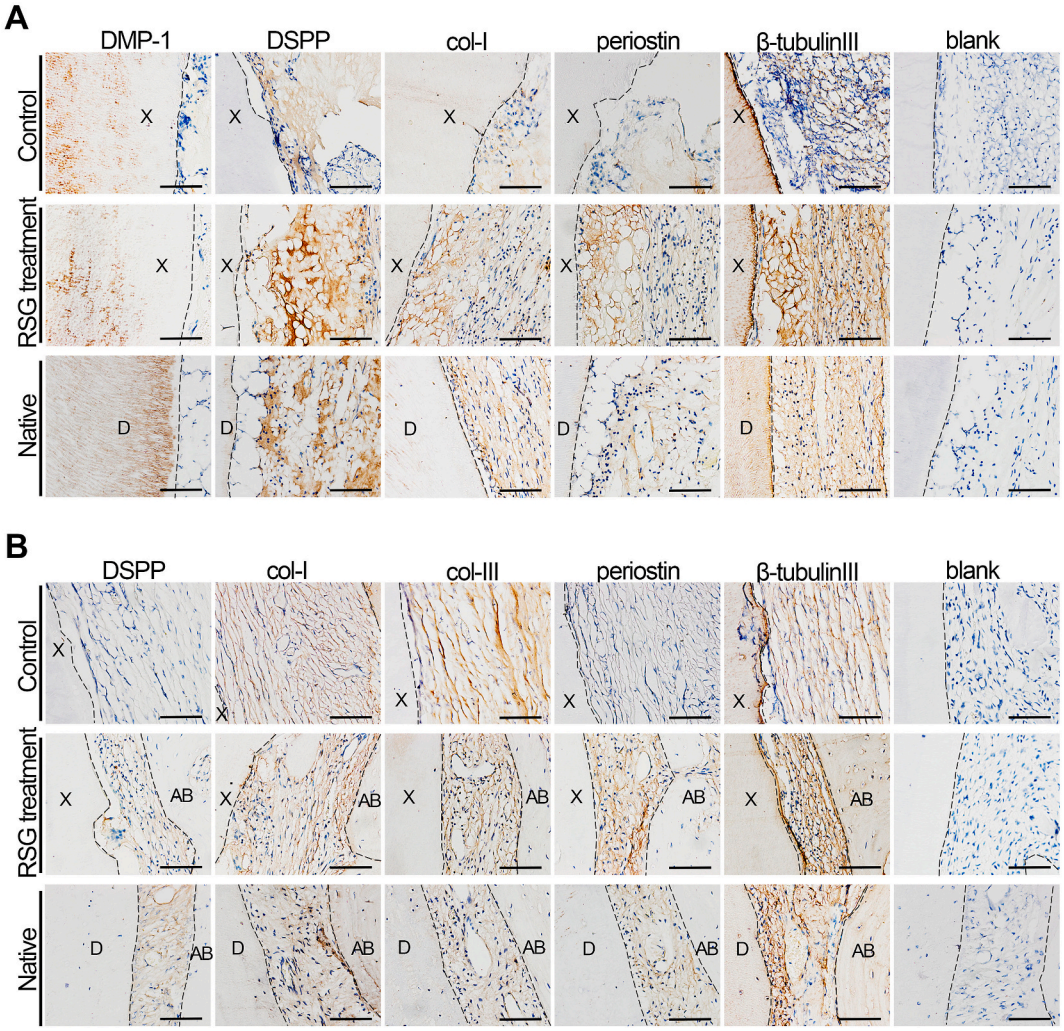

Fig. 7. PPARγ-primed macrophage facilitated functional xenogeneic tooth root regeneration. Odontogenesis-related proteins were evaluated by immunohistochemistry (A) The regenerated pulp-dentin complex-like tissue were positive for dentin marker (DMP-1), odontoblast-related markers (DSPP, periostin), ECM components marker (Col-I), and neuronal marker (β-tubulin III), in line with those of Native. Merely expressed DSPP and periostin were observed in the control group. Scale bars, 100 μm. (B) The regenerated cementum-PDLs-bone complex-like tissue was positive for DSPP, specific PDLs marker (periostin), collagen fibrils marker (Col-I, Col-III), and neuronal marker (β-tubulin III), in line with those of Native. Merely expressed DSPP and periostin were observed in the control group. Scale bars, 100 μm.

responses are immediately initiated with the implantation of ECM-based bioengineered organs. Previous studies did show the recruited M2 macrophage reversely releases enhanced IL-4 and Interleukin 4-induced gene 1 (IL4I1), in return suppressed $CD8^+$ T cells proliferation and Th1 inflammation [37], in line with our findings. And when the $CD4^+$ T cells were co-cultured with M2 polarized peritoneal macrophage, a strong expression of Th2 cytokines would occur, which indeed confirmed the paracrine anti-inflammatory capacities of M2 phenotype [38]. At inflammation sites in situ, M2 phenotypes boost iTreg T cell [39] and inhibit neutrophils infiltration and the oxidative stress [40]. Together these interactions trigger the wound-healing and tissue remodeling process (Fig. 5D and E). Non-degradable ECMs are intendedly implanted with a specific shape like target organs, thus the mechanical stability would be achieved by well-controlled cellular response and limited degradation of M1 macrophages or FBGC [34]. It is required the "right time" for M2 polarization to antagonize this degradation. Meanwhile, fibroblasts are populated at the implantation sites since the initiation of the tissue remodeling process. Via interacting with microenvironmental cues provided by the stable ECM [41], such as strain, stiffness gradients, and topographies, fibroblasts provide deformation fields for oriented collagen fibrils until reaching tensional homeostasis. This normal fiber alignment introduced from fibroblast activities is not sufficient to attract reverse migration of resting macrophage. Recent studies proposed a safe distance between resting macrophage and contractile fibroblasts, since macrophages mechanosense local dynamic force and might migrate towards fibrillar collagen ECM to induce stiff fibrotic ECM-a condition called fibrosis [42]. Consequently, the coordinated activities among macrophage, fibroblast, and ECM could result in integrity of collagen-based tissue remodeling, such as oriented collagen fibrils in regenerated PDLs.

There exists a controversy of the exact macrophage phenotype on promoting mineralization in parenchymal tissues. One view shows that activated inflammatory M1, not M2 macrophages, through a cyclooxygenase-2 (COX2) and prostaglandin-E2 regulatory (PEG2) loop, produce oncostatin M to induce bone formation. Whereas when bone marrow-derived mesenchymal stem cells (MSCs) are co-cultured with monocyte/macrophages, the osteogenic differentiation of MSCs occurs accompanied by $CD206^+$ polarized macrophage [43,44]. Florence Loi et al. recently reported the increased mineralization of preosteoblastic MC3T3 cells was induced during a switch of M1 to M2 macrophages, such as increased alkaline phosphatase (ALP) activity, osteocalcin concentration. and matrix mineralization [45]. The bone impairs/

repair proceed with compositional bone inflammation, absorption, and formation, the timely polarized M2 macrophages display a crucial role in anti-inflammation and bone maturation [43]. Dentine extracellular matrix proteins are similar to bone, consist of the major col-I, acidic proteins, and proteoglycans, these collagenous and non-collagenous proteins create microarchitecture for calcium-phosphate crystal formation. Meanwhile, dentin contains unique proteins different from those in bone and other tissue: DSPP and DMP1 involved in the control of dentin mineralization [46]. The co-culture of human dental pulp cells (DPCs) with M2 conditional medium enhances odontogenic capacities of DPCs, such as increased ALP activity, DSPP expression, and matrix mineralization [47]. Apart from highly expressed DSPP in regenerated pulp and PDL tissues, the timely recruited M2 phenotypes down-regulated expression of MMPs to rescue impaired odontogenesis-related proteins. Several reports have tracked the interaction of MMPs with mineralized dentin, such as MMP1 degrading proteoglycans and collagen while MMP2 degrading DMP1 [48]. Overexpression of MMP1 in PDL cells also causes a significant decrease in Runx 2, osteonectin, osteopontin, bone sialoprotein (BSP), and osteocalcin, which orchestrate odontogenesis, matrix mineralization, cementum formation, and integrity of cementum-PDLs [49]. The polarized M2 macrophage at the early phase in our study timely antagonized MMP1 and MMP2 to contribute to the integrity of cementum-PDLs-bone and dentin re-mineralization, thus effectively supporting biomechanical properties in parenchymal tissues.

Periostin, initially named osteoblast-specific factor 2 (OSF-2), is greatly expressed in collagen-rich connective tissues to mainly maintain the microarchitecture of ECM, such as PDLs [24]. Incisors in periostin-null$^{(-/-)}$ mice showed abnormal remodeling, such as widened PDLs and destruction of alveolar bone, in line with our findings in the control group [24]. We notably reported oriented collagen fibrils, immunostained by periostin, in the RSG treatment group to probably transmit masticatory forces. The highly expressed periostin in PDLs could maintain bone bass and the integrity of the periodontium in response to occlusal loading. The recent study identified PDL-specific isoforms of periostin as essential factors in regulating the differentiation of PDL cells into hard-tissue-forming cells such as cementoblasts and osteoblasts [50], which function in the repair of cementum-PDLs-bone tissue.

How to balance the fibrogenesis process is of tropic interests since excessive ECM depositions also result in fibrosis. Recent studies demonstrated a favorable fate of biomaterial associated with a switch of M1-to-M2 [11]. However, despite a shift to M2 macrophage for xeno-complex was occurred during 3-to-6 weeks xenotransplantation, yet an undesirable fibrous encapsulation was observed at the late phase. Secretive factors from polarized M2 macrophage, such as IL-4, IL-10, and TGF-β1, also participate in fibrosis formation [9]. It is little known of the distinct macrophage phenotype at the healing terminal. Whereas, a part of normal healing tissue is proposed with minimal fibrosis and macrophage deactivation at the late phase [34,51]. We found recruitment of CD206$^+$ macrophage to antagonize inflammation or M1 macrophage at 3 days' xenotransplantation could contribute to functional bioengineered tooth root regeneration. Together, the timely conversion of monocytes/macrophages from a pro-inflammatory to a reparative phenotype is crucial for ECM-based de-novo organogenesis.

M2 macrophages are now expanded into the third set of nomenclature, termed M2a, M2b, and M2c, based upon the inducing agent, molecular marker expression, and functions.[52] M2a activation mainly attenuates proinflammation and releases anti-inflammatory factors, such as IL-10. Macrophages in the mixed pro- and anti-inflammatory markers, termed as M2b phenotype, orchestrating in complements activation and humoral immunity. Then released IL-10 likely stimulates M2c activation, which secrets TGF-β1 and mediates reparative phage. Using this classification system, the macrophage-mediated wound repair is identified as a progression through M1–M2c macrophage activation [53]. The definite functions of these sets in M2-mediated graft immune tolerance warrant further exploration. Furthermore, the short-time M1 infiltration also contributes to the remodeling process, such as angiogenesis. We found accumulated CD31$^+$ endothelial cells at 1week post-implantation of xeno-complexes (without RSG treatment). Blood vessels grow through the process of sprouting, anastomosis, and maturation [20]. M1-secreted factors TNF-α, IL-1β, and VEGF have been shown to promote vessels sprouting by inducing an endothelial tip cell phenotype. While PDGF-BB, TIMP3 secreted from M2a macrophages would recruit pericytes and promote vessel fusion [21]. Therefore, M1-to-M2 macrophage in regulating angiogenesis, especially the effects of timing, deserves more attentions.

5. Conclusion

The present study demonstrated anti-inflammatory, pro-wound-healing, and tissue-regenerating activities of PPARγ-primed CD68$^+$CD206$^+$ macrophage for guiding pulp-dentin and cementum-PDLs-bone regeneration in the xenogeneic bioengineered tooth root. The timely conversion of M1-to-M2 macrophage mainly contributed to balance in fibrogenesis vs fibrosis and bone formation vs absorption, which represents an effective therapeutic target for organ regeneration with compositional parenchymal and stromal tissues.

CRediT authorship contribution statement

Hui Li: Conceptualization, Investigation, Formal analysis, Writing - original draft, Funding acquisition. **Jingjing Sun:** Methodology, Resources, Investigation. **Hefeng Yang:** Investigation, Writing - review & editing. **Xue Han:** Methodology, Investigation. **Xiangyou Luo:** Supervision. **LiJun Liao:** Methodology, Investigation. **Bo Yang:** Methodology, Investigation. **Tian Zhu:** Methodology, Resources. **Fangjun Huo:** Methodology, Investigation. **Weihua Guo:** Conceptualization, Formal analysis, Writing - review & editing, Funding acquisition. **Weidong Tian:** Conceptualization, Formal analysis, Writing - review & editing, Funding acquisition.

Declaration of competing interest

The authors declare that they have no known competing financial interests or personal relationships that could have appeared to influence the work reported in this paper.

Acknowledgments

This work was supported by the National Key Research and Development Program of China (Nos. 2017YFA0104800), Nature Science Foundation of China (31771062, 31971281, 81901001), Key Research and Development Program of Sichuan Province (2017SZ0031).

Appendix A. Supplementary data

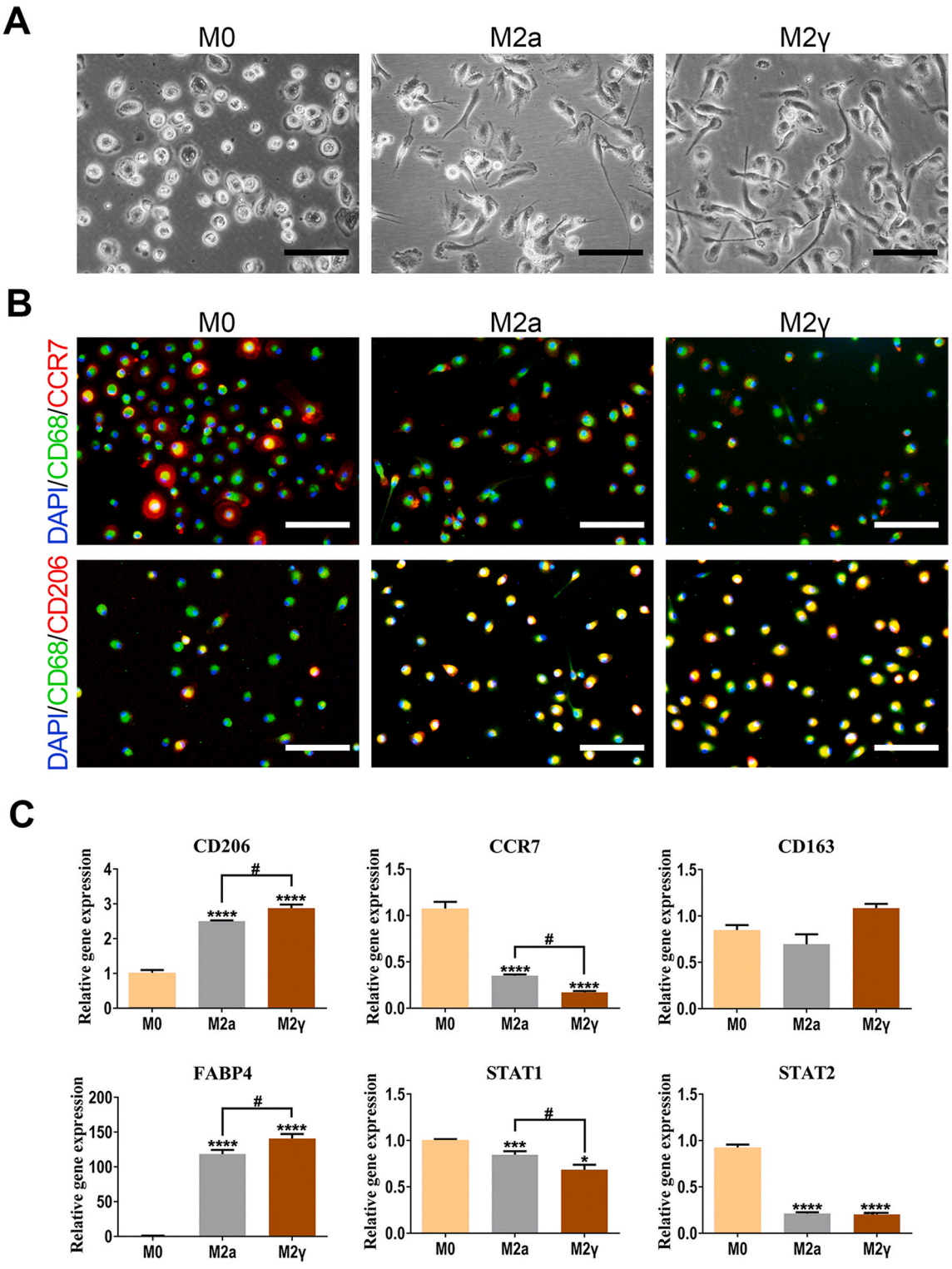

Fig. S1. PPARγ activation augments M2 macrophage polarization in the presence of IL-4 in vitro.

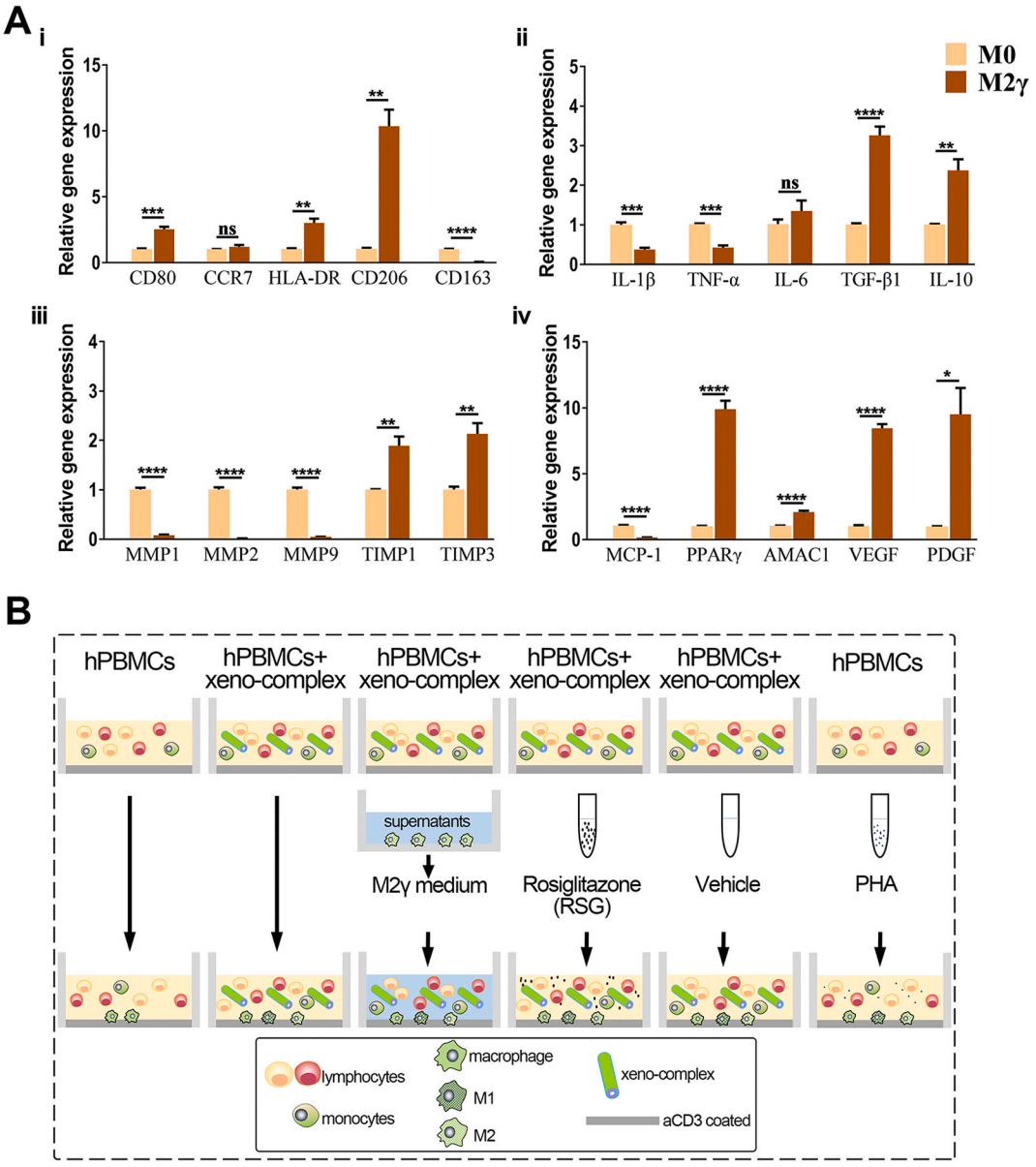

Fig. S2. PPARγ-primed macrophages exhibited anti-inflammatory, tissue-regenerating properties.

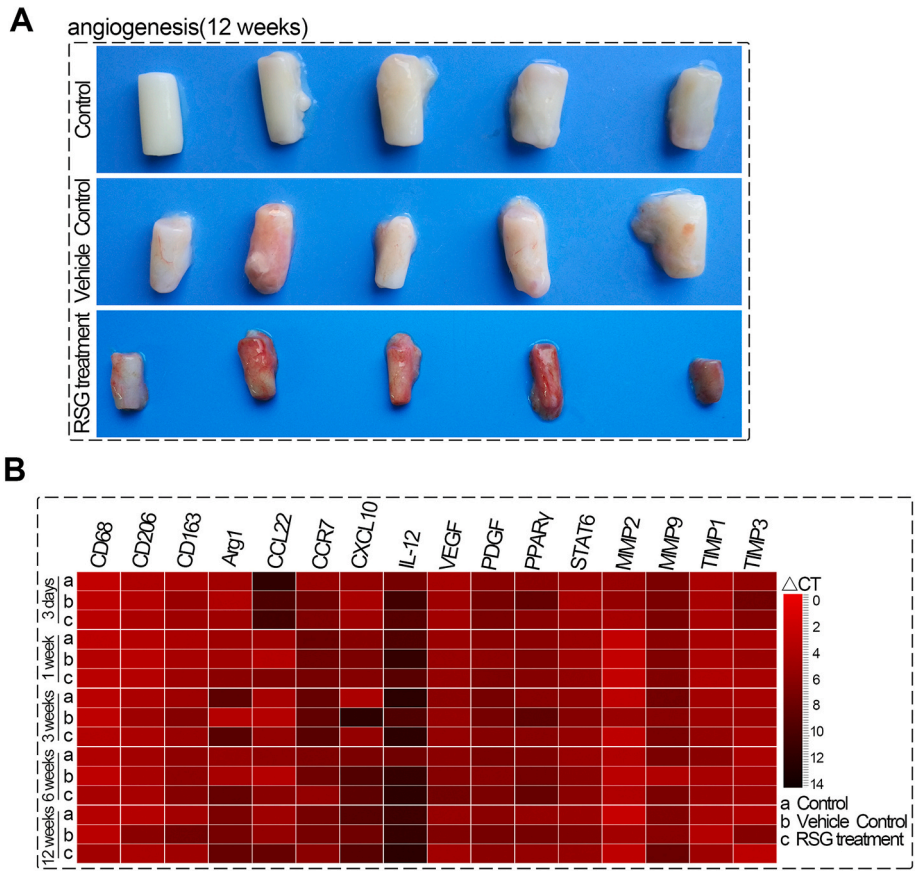

Fig. S3. PPARγ activation augmented vessel infiltration upon xeno-complex.

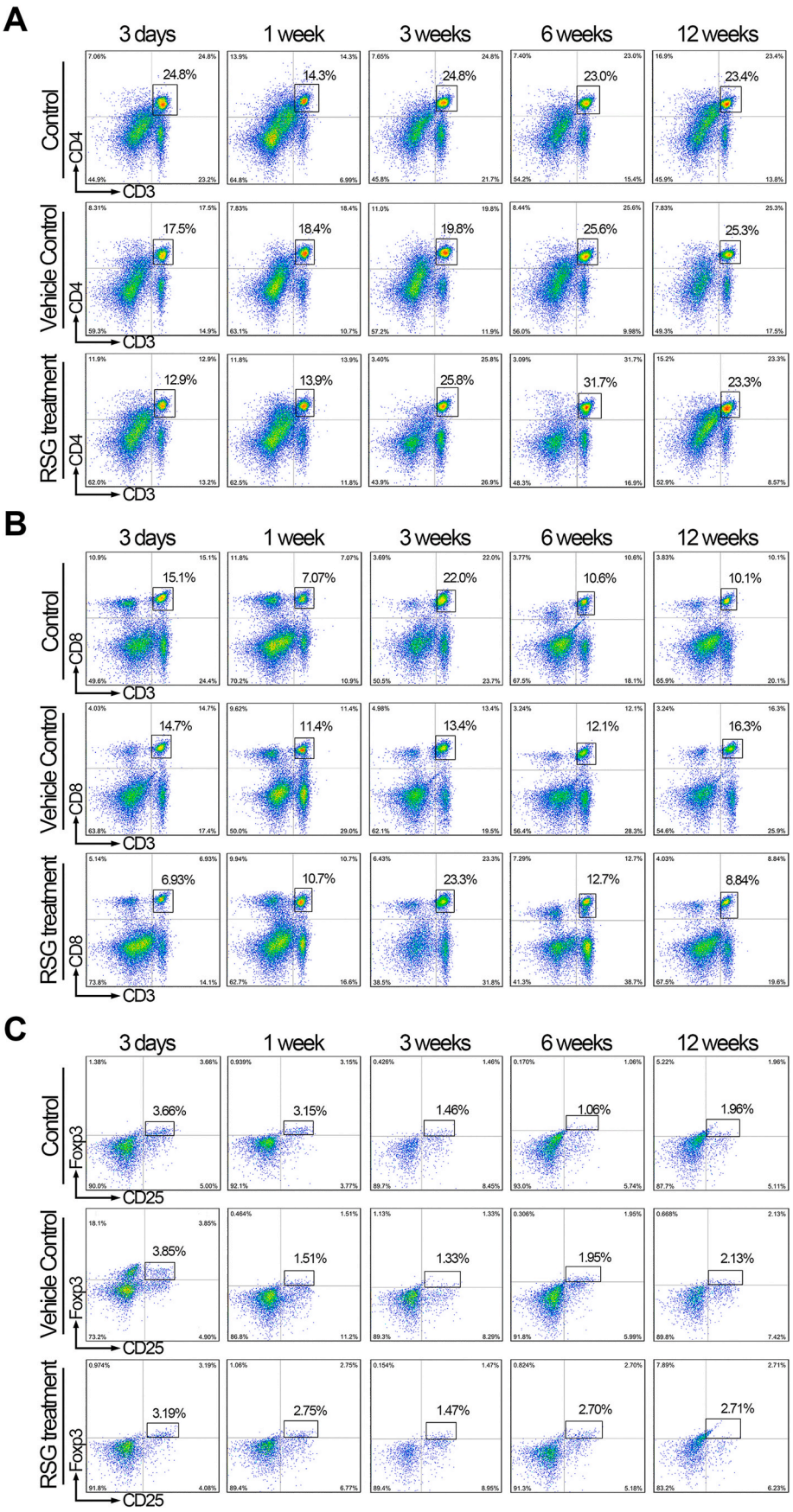

Fig. S4. PPARγ activation inhibited acute T lymphocytes response in the periphery system triggered by xeno-complex.

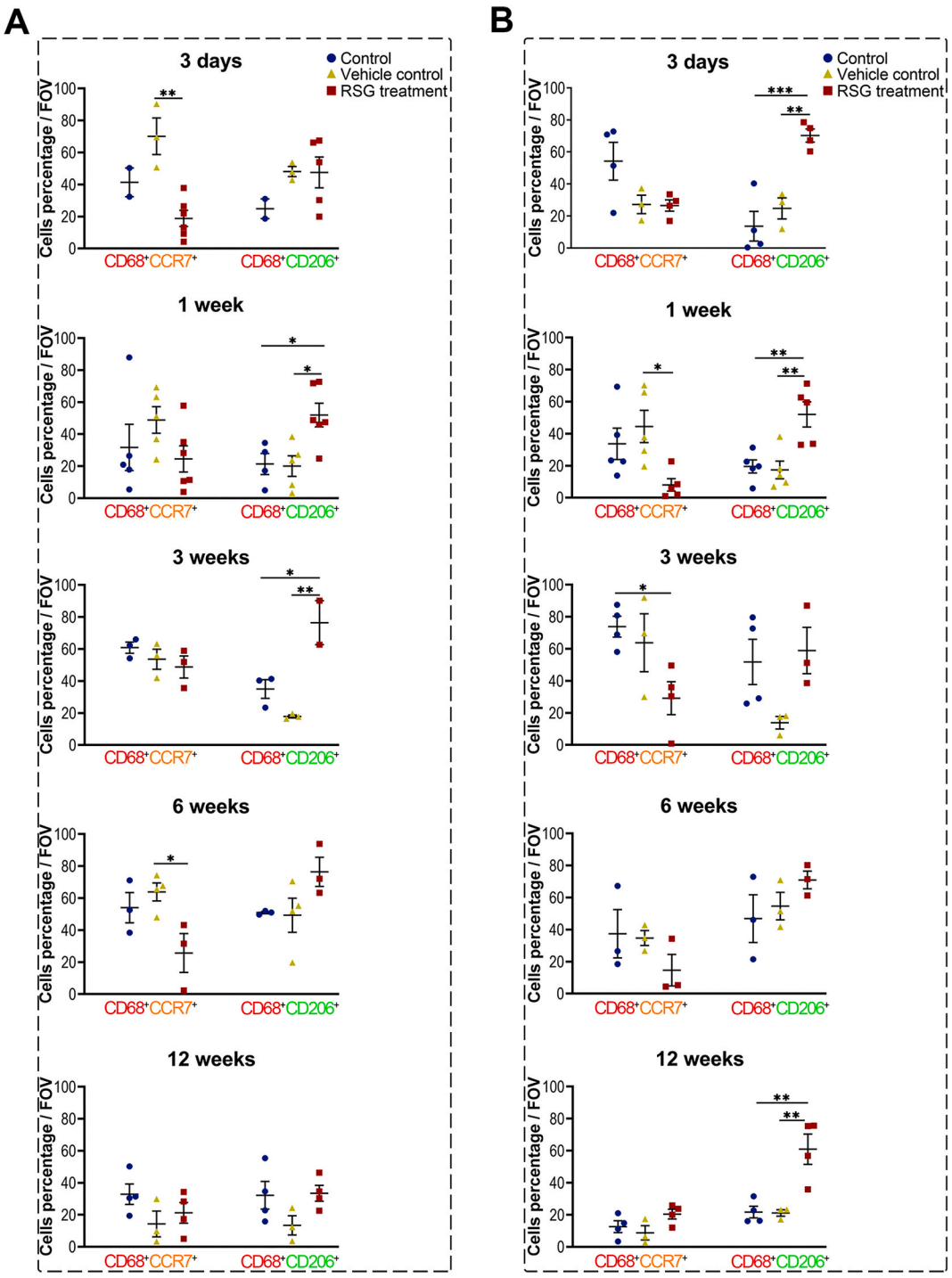

Fig. S5. PPARγ activation recruited CD68^{+}CD206+ tissue macrophage polarization to xeno-complex.

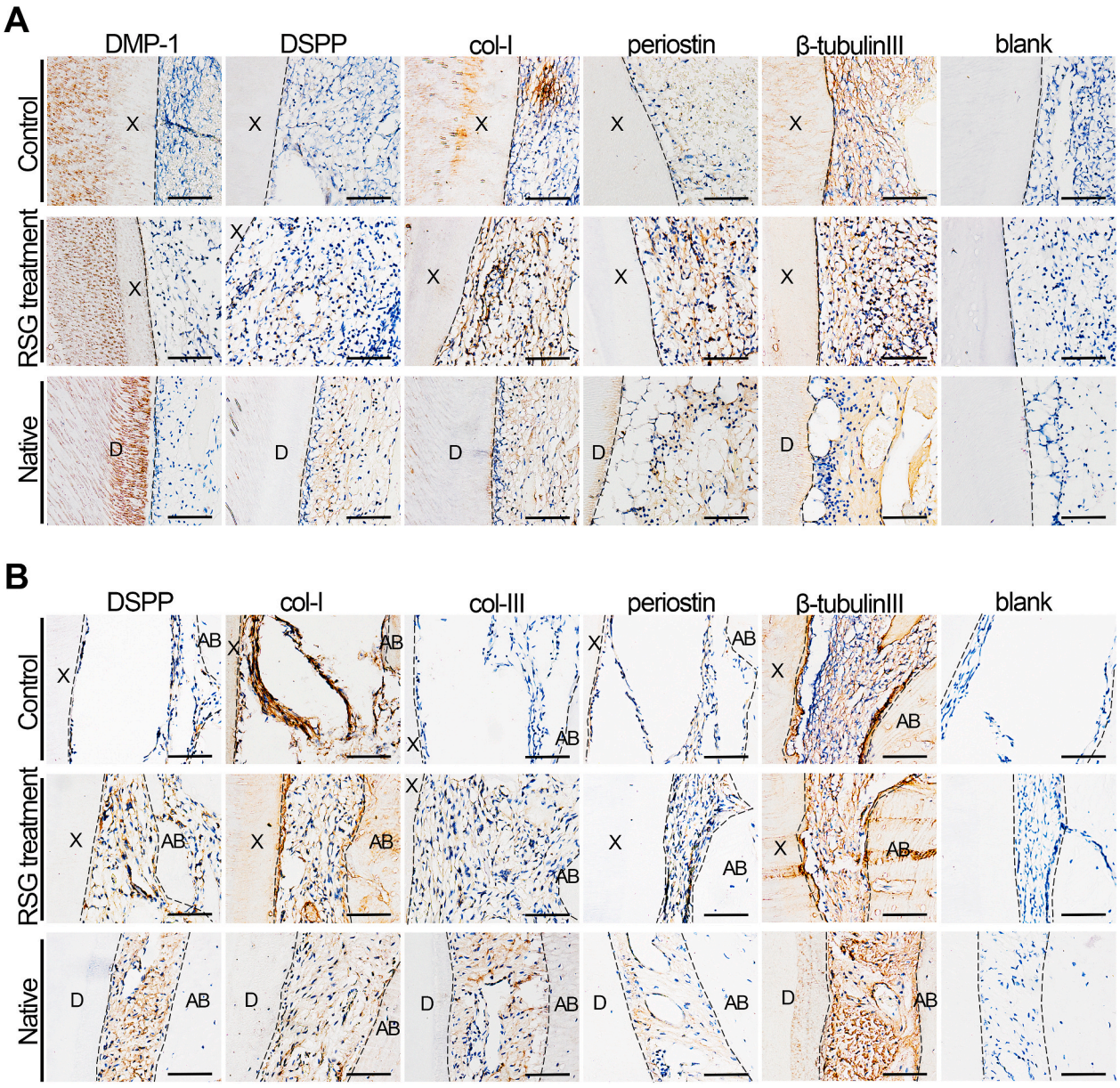

Fig. S6. PPARγ-primed macrophage partially rescued odontogenesis-related proteins at the acute phase.

Appendix B. Supplementary data

Supplementary data to this article can be found online at https://doi.org/10.1016/j.bioactmat.2020.09.029.

References

[1] K.S. Dua, W.J. Hogan, A.A. Aadam, M. Gasparri, In-vivo oesophageal regeneration in a human being by use of a non-biological scaffold and extracellular matrix, Lancet 388 (2016) 55–61, https://doi.org/10.1016/S0140-6736(15)01036-3.

[2] S.F. Badylak, Xenogeneic extracellular matrix as a scaffold for tissue reconstruction, Transpl. Immunol. 12 (2004) 367–377, https://doi.org/10.1016/j.trim.2003.12.016.

[3] D.K. Cooper, Clinical xenotransplantation–how close are we? Lancet 362 (2003) 557–559, https://doi.org/10.1016/S0140-6736(03)14118-9.

[4] L. He, et al., Parenchymal and stromal tissue regeneration of tooth organ by pivotal signals reinstated in decellularized matrix, Nat. Mater. 18 (2019) 627–637, https://doi.org/10.1038/s41563-019-0368-6.

[5] R.M. Wang, et al., Humanized mouse model for assessing the human immune response to xenogeneic and allogeneic decellularized biomaterials, Biomaterials 129 (2017) 98–110, https://doi.org/10.1016/j.biomaterials.2017.03.016.

[6] M.L. Wong, J.L. Wong, N. Vapniarsky, L.G. Griffiths, In vivo xenogeneic scaffold fate is determined by residual antigenicity and extracellular matrix preservation, Biomaterials 92 (2016) 1–12, https://doi.org/10.1016/j.biomaterials.2016.03.024.

[7] D.W. Grainger, All charged up about implanted biomaterials, Nat. Biotechnol. 31 (2013) 507–509, https://doi.org/10.1038/nbt.2600.

[8] M. Karin, H. Clevers, Reparative inflammation takes charge of tissue regeneration, Nature 529 (2016) 307–315, https://doi.org/10.1038/nature17039.

[9] T.A. Wynn, K.M. Vannella, Macrophages in tissue repair, regeneration, and fibrosis, Immunity 44 (2016) 450–462, https://doi.org/10.1016/j.immuni.2016.02.015.

[10] D.M. Mosser, J.P. Edwards, Exploring the full spectrum of macrophage activation, Nat. Rev. Immunol. 8 (2008) 958–969, https://doi.org/10.1038/nri2448.

[11] B.N. Brown, B.D. Ratner, S.B. Goodman, S. Amar, S.F. Badylak, Macrophage polarization: an opportunity for improved outcomes in biomaterials and regenerative medicine, Biomaterials 33 (2012) 3792–3802, https://doi.org/10.1016/j.biomaterials.2012.02.034.

[12] F. Kano, K. Matsubara, M. Ueda, H. Hibi, A. Yamamoto, Secreted ectodomain of sialic acid-binding Ig-like lectin-9 and monocyte chemoattractant protein-1 synergistically regenerate transected rat peripheral nerves by altering macrophage polarity, Stem Cell. 35 (2017) 641–653, https://doi.org/10.1002/stem.2534.

[13] S.S. Jin, et al., A biomimetic hierarchical nanointerface orchestrates macrophage polarization and mesenchymal stem cell recruitment to promote endogenous bone

regeneration, ACS Nano 13 (2019) 6581–6595, https://doi.org/10.1021/acsnano.9b00489.
[14] H. Li, et al., Xenogeneic bio-root prompts the constructive process characterized by macrophage phenotype polarization in rodents and nonhuman primates, Adv. Healthc. Mater. 6 (2017), https://doi.org/10.1002/adhm.201601112.
[15] R. Li, et al., Human treated dentin matrix as a natural scaffold for complete human dentin tissue regeneration, Biomaterials 32 (2011) 4525–4538, https://doi.org/10.1016/j.biomaterials.2011.03.008.
[16] A. Bayrak, et al., Human immune responses to porcine xenogeneic matrices and their extracellular matrix constituents in vitro, Biomaterials 31 (2010) 3793–3803, https://doi.org/10.1016/j.biomaterials.2010.01.120.
[17] M.A. Bouhlel, et al., PPARgamma activation primes human monocytes into alternative M2 macrophages with anti-inflammatory properties, Cell Metabol. 6 (2007) 137–143, https://doi.org/10.1016/j.cmet.2007.06.010.
[18] C.J. Villanueva, P. Tontonoz, Licensing PPARgamma to work in macrophages, Immunity 33 (2010) 647–649, https://doi.org/10.1016/j.immuni.2010.11.017.
[19] G. Pascual, et al., A SUMOylation-dependent pathway mediates transrepression of inflammatory response genes by PPAR-gamma, Nature 437 (2005) 759–763, https://doi.org/10.1038/nature03988.
[20] S.P. Herbert, D.Y. Stainier, Molecular control of endothelial cell behaviour during blood vessel morphogenesis, Nat. Rev. Mol. Cell Biol. 12 (2011) 551–564, https://doi.org/10.1038/nrm3176.
[21] K.L. Spiller, et al., The role of macrophage phenotype in vascularization of tissue engineering scaffolds, Biomaterials 35 (2014) 4477–4488, https://doi.org/10.1016/j.biomaterials.2014.02.012.
[22] X. Luo, et al., CAD based design sensitivity analysis and shape optimization of scaffolds for bio-root regeneration in swine, Biomaterials 57 (2015) 59–72, https://doi.org/10.1016/j.biomaterials.2015.03.062.
[23] K. Narayanan, et al., Differentiation of embryonic mesenchymal cells to odontoblast-like cells by overexpression of dentin matrix protein 1, Proc. Natl. Acad. Sci. U. S. A. 98 (2001) 4516–4521, https://doi.org/10.1073/pnas.081075198.
[24] G.E. Romanos, K.P. Asnani, D. Hingorani, V.L. Deshmukh, PERIOSTIN: role in formation and maintenance of dental tissues, J. Cell. Physiol. 229 (2014) 1–5, https://doi.org/10.1002/jcp.24407.
[25] W. Guo, et al., The use of dentin matrix scaffold and dental follicle cells for dentin regeneration, Biomaterials 30 (2009) 6708–6723, https://doi.org/10.1016/j.biomaterials.2009.08.034.
[26] W. Guo, et al., Dental follicle cells and treated dentin matrix scaffold for tissue engineering the tooth root, Biomaterials 33 (2012) 1291–1302, https://doi.org/10.1016/j.biomaterials.2011.09.068.
[27] L. Luo, et al., Potential roles of dental pulp stem cells in neural regeneration and repair, Stem Cell. Int. (2018) 1731289, https://doi.org/10.1155/2018/1731289.
[28] X. Chen, et al., Notch 1 signaling regulates the proliferation and self-renewal of human dental follicle cells by modulating the G1/S phase transition and telomerase activity, PLoS One 8 (2013) e69967, , https://doi.org/10.1371/journal.pone.0069967.
[29] J.M. Fishman, et al., Immunomodulatory effect of a decellularized skeletal muscle scaffold in a discordant xenotransplantation model, Proc. Natl. Acad. Sci. U. S. A. 110 (2013) 14360–14365, https://doi.org/10.1073/pnas.1213228110.
[30] A.S. Shaw, E.L. Filbert, Scaffold proteins and immune-cell signalling, Nat. Rev. Immunol. 9 (2009) 47–56, https://doi.org/10.1038/nri2473.
[31] M.M.P. Alvarez, et al., PAR-1 and PAR-2 expression is enhanced in inflamed odontoblast cells, J. Dent. Res. 96 (2017) 1518–1525, https://doi.org/10.1177/0022034517719415.
[32] H. Xu, et al., Multiple essential MT1-MMP functions in tooth root formation, dentinogenesis, and tooth eruption, Matrix Biol. 52–54 (2016) 266–283, https://doi.org/10.1016/j.matbio.2016.01.002.
[33] M.C. Cramer, S.F. Badylak, Extracellular matrix-based biomaterials and their influence upon cell behavior, Ann. Biomed. Eng. 48 (2020) 2132–2153, https://doi.org/10.1007/s10439-019-02408-9.
[34] R. Klopfleisch, Macrophage reaction against biomaterials in the mouse model - phenotypes, functions and markers, Acta Biomater. 43 (2016) 3–13, https://doi.org/10.1016/j.actbio.2016.07.003.
[35] L. Huleihel, et al., Macrophage phenotype in response to ECM bioscaffolds, Semin. Immunol. 29 (2017) 2–13, https://doi.org/10.1016/j.smim.2017.04.004.
[36] A. Petrosyan, et al., A step towards clinical application of acellular matrix: a clue from macrophage polarization, Matrix Biol. 57–58 (2017) 334–346, https://doi.org/10.1016/j.matbio.2016.08.009.
[37] Y. Yue, et al., IL4I1 is a novel regulator of M2 macrophage polarization that can inhibit T cell activation via L-tryptophan and arginine depletion and IL-10 production, PLoS One 10 (2015) e0142979, , https://doi.org/10.1371/journal.pone.0142979.
[38] S. Oishi, et al., M2 polarization of murine peritoneal macrophages induces regulatory cytokine production and suppresses T-cell proliferation, Immunology 149 (2016) 320–328, https://doi.org/10.1111/imm.12647.
[39] D. Haribhai, et al., Alternatively activated macrophages boost induced regulatory T and Th17 cell responses during Immunotherapy for colitis, J. Immunol. 196 (2016) 3305–3317, https://doi.org/10.4049/jimmunol.1501956.
[40] F. Wang, et al., Bone marrow derived M2 macrophages protected against lipopolysaccharide-induced acute lung injury through inhibiting oxidative stress and inflammation by modulating neutrophils and T lymphocytes responses, Int. Immunopharm. 61 (2018) 162–168, https://doi.org/10.1016/j.intimp.2018.05.015.
[41] M.S. Hall, et al., Fibrous nonlinear elasticity enables positive mechanical feedback between cells and ECMs, Proc. Natl. Acad. Sci. U. S. A. 113 (2016) 14043–14048, https://doi.org/10.1073/pnas.1613058113.
[42] P. Pakshir, et al., Dynamic fibroblast contractions attract remote macrophages in fibrillar collagen matrix, Nat. Commun. 10 (2019) 1850, https://doi.org/10.1038/s41467-019-09709-6.
[43] J. Pajarinen, et al., Mesenchymal stem cell-macrophage crosstalk and bone healing, Biomaterials 196 (2019) 80–89, https://doi.org/10.1016/j.biomaterials.2017.12.025.
[44] N.J. Horwood, Macrophage polarization and bone formation: a review, Clin. Rev. Allergy Immunol. 51 (2016) 79–86, https://doi.org/10.1007/s12016-015-8519-2.
[45] F. Loi, et al., The effects of immunomodulation by macrophage subsets on osteogenesis in vitro, Stem Cell Res. Ther. 7 (2016) 15, https://doi.org/10.1186/s13287-016-0276-5.
[46] A. Linde, The extracellular matrix of the dental pulp and dentin, J. Dent. Res. 64 (1985) 523–529, https://doi.org/10.1177/00220345885064004O5 Spec No.
[47] H.C. Park, et al., The effects of M1 and M2 macrophages on odontogenic differentiation of human dental pulp cells, J. Endod. 43 (2017) 596–601, https://doi.org/10.1016/j.joen.2016.11.003.
[48] C. Chaussain, et al., MMP2-cleavage of DMP1 generates a bioactive peptide promoting differentiation of dental pulp stem/progenitor cell, Eur. Cell. Mater. 18 (2009) 84–95, https://doi.org/10.22203/ecm.v018a08.
[49] T. Hayami, Y.L. Kapila, S. Kapila, MMP-1 (collagenase-1) and MMP-13 (collagenase-3) differentially regulate markers of osteoblastic differentiation in osteogenic cells, Matrix Biol. 27 (2008) 682–692, https://doi.org/10.1016/j.matbio.2008.07.005.
[50] S. Yamada, et al., Characterization of a novel periodontal ligament-specific periostin isoform, J. Dent. Res. 93 (2014) 891–897, https://doi.org/10.1177/0022034514543015.
[51] M.L. Novak, T.J. Koh, Phenotypic transitions of macrophages orchestrate tissue repair, Am. J. Pathol. 183 (2013) 1352–1363, https://doi.org/10.1016/j.ajpath.2013.06.034.
[52] P.J. Murray, et al., Macrophage activation and polarization: nomenclature and experimental guidelines, Immunity 41 (2014) 14–20, https://doi.org/10.1016/j.immuni.2014.06.008.
[53] A. Mantovani, et al., The chemokine system in diverse forms of macrophage activation and polarization, Trends Immunol. 25 (2004) 677–686, https://doi.org/10.1016/j.it.2004.09.015.